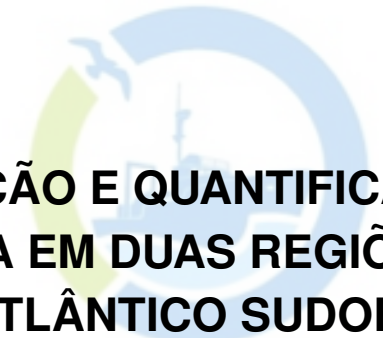RAFAEL ANDRÉ ÁVILA

CARACTERIZAÇÃO E QUANTIFICAÇÃO DA MISTURA TURBULENTA EM DUAS REGIÕES DO OCEANO ATLÂNTICO SUDOESTE

Tese submetida ao *Programa de pós-graduação em oceanografia física, química e geológica* do Instituto de Oceanografia da Universidade Federal do Rio Grande como requisito parcial para a obtenção do titulo de doutor em oceanografia física, química e geológica

Orientador: Paulo Henrique Rezende Calil

RAFAEL ANDRÉ ÁVILA

CHARACTERIZATION AND QUANTIFICATION OF TURBULENT MIXING IN TWO REGIONS OF THE SOUTHWESTERN ATLANTIC OCEAN

Ph.D. Thesis

Supervisor: Paulo Henrique Rezende Calil

Agradecimentos

'When I meet God, I'm going to ask Him two questions: why relativity? And why turbulence? I really believe He'll have an answer for the first.'

Werner Heisenberg

CHARACTERIZATION AND QUANTIFICATION OF TURBULENT MIXING IN TWO REGIONS OF THE SOUTHWESTERN ATLANTIC OCEAN

by

Rafael André Ávila

Abstract

The Southern Brazilian Shelf and The Vitória-Trindade Ridge are two important regions in the southwestern Atlantic Ocean, which were previously investigated in terms of circulation and dynamics, and the respective implications in the local physical and biological responses. However, these areas have never been characterized in terms of turbulent mixing, which would contribute significantly to the knowledge of their dynamics and the overall implications in the southwestern Atlantic Ocean circulation.

This thesis presents the first turbulence observations in these important regions, with the objective of characterizing their turbulent mixing pattern and quantifying its magnitude. Results in the Southern Brazilian Shelf demonstrated the importance of the La Plata River plume in inhibiting vertical mixing in the continental shelf and suggested that this large-scale plume has a dynamic mid-field region. The survey in the Vitória Trindade Ridge shows that this region is a potential hot spot for mixing, as the local circulation interacts with topographic features to yield surface and subsurface turbulent mixing. Results also suggest that internal tides are prone to occur and may induce enhanced turbulence at subsurface levels.

Results herein are an initial contribution for the characterization and quantification of turbulence processes in the southwestern Atlantic Ocean. This thesis expects to provide a base for future studies and contribute to the understanding of the overall mixing pattern and the respective implications in those regions.

CARACTERIZAÇÃO E QUANTIFICAÇÃO DA MISTURA TURBULENTA EM DUAS REGIÕES DO OCEANO ATLÂNTICO SUDOESTE

por

Rafael André Ávila

Resumo

A Plataforma Continental Sul-Brasileira e a Cadeia Vitória-Trindade são duas regiões importantes no Oceano Atlântico Sudoeste que foram previamente investigadas em termos de circulação e dinâmica, além das possíveis consequências nas respostas físico-biológicas locais. Entretanto, ambas as regiões nunca foram caracterizadas em termos de mistura turbulenta, a qual forneceria uma contribuição importante acerca do conhecimento desses locais e das possíveis implicações na dinâmica do Oceano Atlântico Sudoeste.

Nesta tese estão apresentadas as primeiras observações de turbulência de microestrutura nestas regiões, com o objetivo de caracterizar o padrão de mistura turbulenta e quantificar sua magnitude. Os resultados na Plataforma Continental Sul-Brasileira demonstram a importância da pluma do Rio da Prata em inibir a mistura vertical nessa plataforma continental dinâmica e também sugerem a presença de uma região dinâmica intermediária na pluma quando esta se aproxima da quebra de plataforma. Os resultados obtidos na Cadeia Vitória-Trindade demonstram que a região é um "hot-spot" de mistura devido às interações do escoamento com a complexa batimetria local, além de ser um local propenso à geração de mistura turbulenta em subsuperfície devido à ocorrência de marés internas.

Os resultados aqui obtidos representam uma contribuição inicial para o entendimento dos processos de mistura turbulenta no Oceano Atlântico Sudoeste. Esta tese visa prover uma base para futuros estudos e contribuir para a compreensão dos processos de turbulência nessas importantes regiões.

Contents

---

[1]Parte do Programa de Recursos Humanos (PRH-27) - Petrobrás e Agência Nacional do Petróleo

List of Figures

Acronyms

BC Brazil Current

BCC Brazilian Coastal Current

DDC double-diffusive convection

DR diffusive regime

KH Kelvin-Helmholtz

LHS left-hand side

OI ocean interior

PPW Plata Plume Water

RHS right-hand side

SACW South Atlantic Central Water

SBS Southern Brazilian Shelf

SFR salt-finger regime

SML surface mixed layer

STSW Subtropical Shelf Water

TKE turbulent kinetic energy

TS temperature-salinity

TW Tropical Water

VTR Vitória-Trindade Ridge

Chapter 1

Turbulence in the ocean

1.1 Introduction

According to Rick Salmon in his book (Salmon, 1998), there is not a clear definition of what turbulence is. He quotes: "Every aspect of turbulence is controversial. Even the definition of fluid turbulence is a subject of disagreement". It is a process constituted of several properties and one of the most important is that turbulence increases the effectiveness of transferring momentum mass and heat in rotating and non-rotating fluids. It occurs as a consequence of random fluctuations yielded by forces that induce instabilities in the dynamics of a moving flow, generating a highly energetic state capable of stirring and mixing and generate strong property gradients at relatively small

spatial scales.

Turbulent flow may be succinctly defined as a disorganized fluid motion. Pioneering experiments were performed by Osborne Reynolds in the late nineteenth century based on his studies on flows in water pipes. At sufficiently low flow speed U_0 in pipes of diameter d, Reynolds observed that dyed fluid particles followed straight line paths parallel to the pipe wall, in what is referred as laminar flow. As U_0 and d increased, an abrupt transition in flow regime occurred at a certain point, in which fluid particles no longer stayed on wall-parallel streamlines, acquiring random components of velocity both across and along the pipe axis, acquiring the characteristics of what became known as turbulent flow. Based on these observations, Reynolds deduced that the transition between laminar and turbulent conditions is controlled by the relative magnitude of inertial and viscous forces, which can be expressed by a non-dimensional number, the Reynolds number,

$$Re = \frac{U_0 d}{\nu}, \tag{1.1}$$

where ν is the kinematic viscosity of the fluid. Experiments showed that for values of Re greater than $\sim$2000, the flow was turbulent and a tracer, introduced at a certain point into the flow, was rapidly diffused across the pipe section by turbulent components in the flow. Reynolds experiment may be considered the first and one of the most important steps in the study of turbulence in fluid dynamics, and the Reynolds number is used as a parameter to define flow conditions up to today.

The motion of a turbulent flow can be described as a combination of eddies of different scales, and it is the overlying effect of these eddies that is responsible for the random nature of turbulence. Two distinct particles in a turbulent flow tend to separate from each other rapidly due to dispersion. In a laminar flow, where the transfer of fluid properties is limited to molecular diffusion, the dispersion is generally a very slow process when compared to a turbulent flow. Molecular diffusion is governed by Fick's law[1], in which the flux J of a given fluid is related to the gradient of its concentration,

$$J = -k_m \frac{\partial c}{\partial \eta}, \tag{1.2}$$

where k_m is the molecular diffusivity, usually a very small quantity, and $\partial c/\partial \eta$ is the gradient of concentration of a given property. For example, Simpson and Sharples (2012) estimate that, If there is no turbulence in a shelf sea of depth $h = 100$ m, and all heat exchange is through molecular diffusion, it would take about h^2/k_m $\sim$2260 years to achieve equilibrium. Turbulent motion is much more efficient in mixing, reducing this

---

[1]This is related to Fick's first law, which postulates that the flux goes from regions of high concentration to regions of low concentration, with a magnitude that is proportional to the concentration gradient, assuming a steady state (Kundu et al., 2001).

time scale to, approximately, one year.

Turbulence increases the efficiency of stirring and mixing in fluids, and in the study of turbulence it is important to distinguish both and know how they are linked to the turbulent motion. Stirring is the addition of mechanical energy into the flow, while mixing is the process of mingling the properties of the fluid. Stirring and mixing are related to turbulence by stretching out the interface between the fluid and particles, creating a larger interface area and increasing spatial gradients. The process of distortion due to turbulence is graphically depict in figure 1.1. Stirring extends the surface of contact between fluid volumes or, in the case of the example, the length of the lines between the black and white areas in the checkerboard. Clearly, the example in the figure does not depicts mixing, but the stretching produced by tangential forces within a eddying flow field, which eventually leads to a more efficient mixing. Stirring and mixing occur naturally in fluids motion, but are faster and much more effective when turbulence is involved.

One of the most important characteristics of turbulence is it dissipative nature, which converts the kinetic energy of the motion into heat (Thorpe, 2007). The energy carried out from larger spatial scales is progressively transferred to smaller scales where molecular viscosity becomes important relative to the mean flow, and the relatively large velocity gradients result in large Reynolds stress[2], converting the kinetic energy of turbulent eddies into heat. The Reynolds stress can be expressed by the stress law for molecular viscosity,

$$\tau = -\rho\nu\frac{\partial u}{\partial \eta},\tag{1.3}$$

where the stress τ is parallel to the flow direction and $\partial u/\partial \eta$ is the velocity gradient normal to the flow. Energy may also be consumed by turbulence in mixing a stratified fluid, in which work is being made in moving fluid across vertical density gradients, or upward against gravity. If the energy supply is insufficient to work against stratification, turbulence will not be maintained and will fade away.

Turbulence is quantified by the rate of dissipation of turbulent kinetic energy (hereafter TKE), or ϵ, which is the rate of kinetic energy being converted into heat due to viscous friction, with units of energy per second per mass. More details about ϵ are presented in section 1.3.

The role of turbulence in the ocean dynamics is to act as an moderator to the large-scale motions preventing the exponential increase of energy by extracting and redistributing momentum and transferring the energy through the ocean energy cascade towards the small scales. The energy cascade is the transfer of TKE from the

---

[2]The Reynolds stress, referred by the letter τ, is a factor that determines the nature of the dynamics of the oceanic boundary layers. It describes the tangential forces acting upon laminar fluxes that will eventually become unstable, leading to mixing.
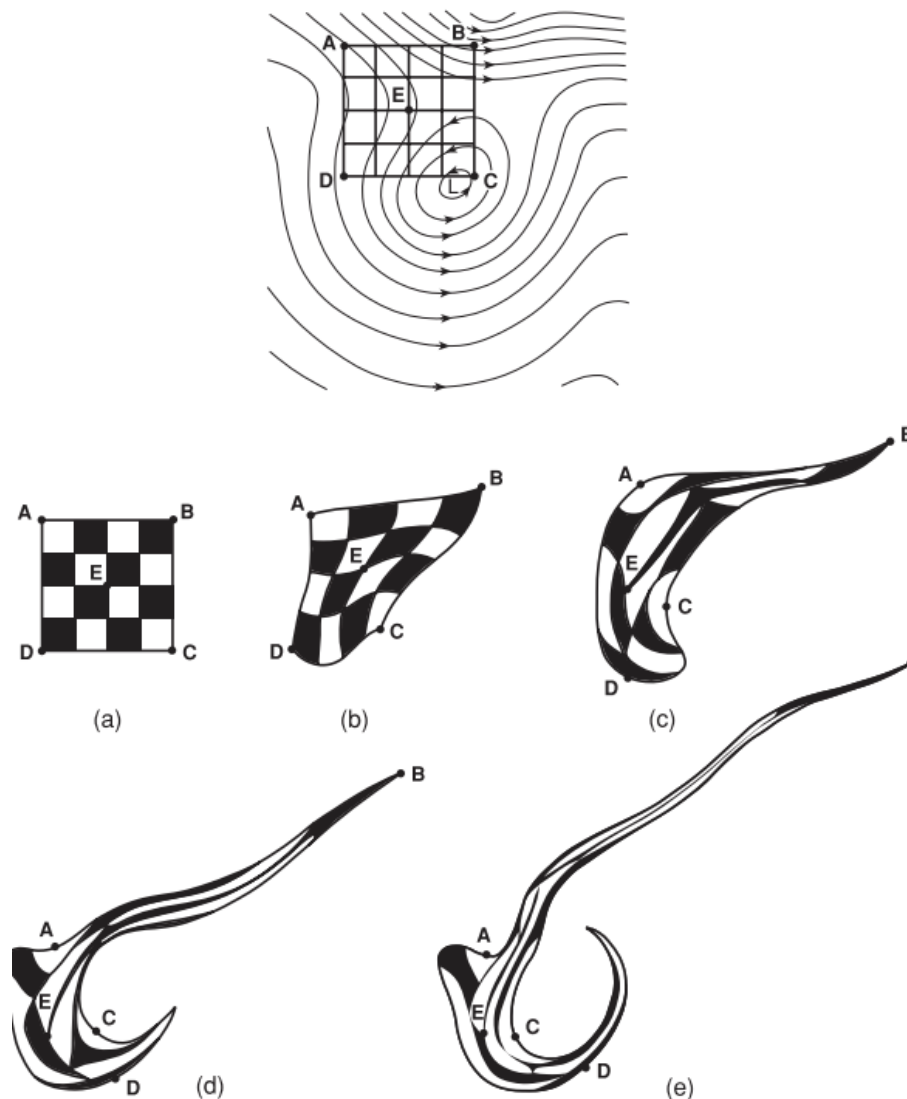
Fig. 1.1: The distortion of a checkerboard pattern due to an eddy motion. The stages of distortion are shown from (a) to (e), and each location of points A, B, C, D and E indicate their dispersion relative to the first stage. From Thorpe (2007).

low wavenumbers, or large spatial scales, which is where the energy is injected, to the high wavenumbers, or small spatial scales, where the energy is dissipated by viscous friction. In the intermediate range of scales, the inertial subrange, energy can not be dissipated, added or removed, only transferred.

The largest turbulent eddies contain most of the kinetic energy, whereas the smallest eddies, characterized by velocity fluctuations, are responsible for the dissipation of TKE in the dissipation scales. Turbulence is assumed to be isotropic and homogeneous in the mid-range between the scale of the largest and the smallest turbulent eddies, based on the hypotheses of Andrey Kolmogorov (Kolmogorov, 1968)[3] and Geoffrey Taylor (Tennekes and Lumley, 1972).

[3]*Reprinted from Dokl. Akad. Nauk SSSR 30, 299 (1941), Submitted originally December 28, 1940.

Dissipation can be expressed in terms of fluctuations in the rate of strain of the turbulent flow and the fluid's kinematic viscosity, ν[4]. However, the fluctuations are a property of the flow, not the fluid, which leads to a closure problem (Cushman-Roisin and Beckers, 2011), addressed in section 1.3.2.

In oceanic flows, stratification plays a key role on turbulence generation and maintenance, as it acts against the effects of turbulent mixing. Atmospheric heating and the ensuing heat distribution by the ocean's circulation, as well as the freshwater inputs in coastal seas result in strong variations in the density distribution that affect greatly the mixing pattern in the ocean. Stratification prevents instability and vertical mixing due to buoyancy effects. A strong and stable thermocline, for instance, inhibits exchanges between upper and lower layers of fluid, thus requiring energy input from a turbulent agent to weaken the stratification and induce instability. As usually observed in the ocean, the vertical density profile, $d\rho/dz$, is negative, i.e., density increases with depth (assuming the depth z as negative below the sea surface), which is unlikely to generate turbulence. However, when $d\rho/dz$ is positive, it may lead to the growth of vertical disturbances and/or convection and increasing instabilities, which may lead to TKE dissipation. Stratification may lead to instabilities when shear occurs at density interfaces and induce variations on the vertical density profile. The tendency toward instability in a shear-stratified flow is given by the gradient Richardson number

$$Ri_g = \frac{N^2}{S^2},\qquad(1.4)$$

where N^2 is the squared buoyancy (or Brunt-Väisälä) frequency and S^2 represents an energy source for instability, being usually expressed by the squared vertical velocity shear, $(\partial v/\partial z)^2$. N is the strength of stratification, given by

$$N = \sqrt{-\frac{g}{\rho_0}\frac{\partial\rho}{\partial z}},\qquad(1.5)$$

where g is the acceleration of gravity and ρ_0 is the average density[5]. The buoyancy frequency characterizes the highest frequencies of free small amplitude oscillations that occur naturally in a stably stratified fluid. Values of Ri_g smaller than 0.25, obtained in laboratory experiments, indicate tendency towards unstable conditions, which are associated with Kelvin-Helmholtz (KH) instabilities (De Silva et al., 1996). Through this instability, the inertial shear is concentrated into discrete eddies, namely the KH billows, with axes aligned horizontally and perpendicular to the flow. The billows eventually

---

[4]The kinematic viscosity or momentum diffusivity, is the ratio of the dynamic viscosity, μ, to the density of the fluid, ρ. For large scales motions, the viscous friction terms in the momentum equations have different magnitude for horizontal and vertical directions. At small scales, however, viscous forces have similar magnitude for the three spatial components (Kundu et al., 2001).

[5]The average density of seawater is 1023.6 kgm^3, at 1 atm of pressure, temperature of 25℃, salinity of 35 PSU.

overturn and generate small-scale turbulence and mixing at stratified interfaces (Lamb, 2014).

1.2 Turbulence generation in the ocean

As the ocean is intrinsically turbulent, the knowledge of turbulence processes is crucial to understand and describe accurately the ocean dynamics and build reliable numerical models that forecast the ocean behavior. The density stratification at different parts of the ocean is related to the local processes that lead to turbulence. Stratification effectively divides the ocean into zones of different turbulence characteristics, and this division is used to discriminate between the turbulence in the surface and benthic layers, and the turbulence in the ocean interior, due to processes that occur at stratified interfaces. Unlikely the rapid transition described by Reynolds, the transition from laminar flow to turbulence resulting from KH instabilities occurs relatively slow through a set of distinct stages

1.2.1 Turbulence processes in the boundary layers

The effect of turbulence in the ocean is most effective at its boundaries (Gargett, 1989), being (1) the upper ocean layer or region near the sea surface that is directly affected by the overlying atmosphere, and (2) the benthic or bottom boundary layer that lies above the underlying solid seabed. At these two layers, air-sea interaction and bottom friction, respectively, act to increase velocity shear and, therefore, generate mixing. At the surface layer, heat fluxes add or remove buoyancy, leading to convective mixing due to density adjustments. In addition, the freshwater inputs from nearby rivers or estuaries, rain and snow also affect the local buoyancy. At the surface, wind stress has a very important role on turbulence, as it induces velocity shear and generate waves. At the bottom layer, atmospheric process are usually of low relevance (except at very shallow shelf regions), being the friction upon seabed flows the responsible for TKE production.

Much of the turbulence induced at the surface and bottom boundary layers is caused by processes resulting from the fluxes of buoyancy and momentum through the nearby boundary, and these are defined as external processes, driven by sources of energy outside the boundary layers. The wind-driven breaking waves and convection produced by air-sea buoyancy flux are examples of external processes, as well as the stress exerted by a seabed on a flow close to the bottom. Alternatively, processes that lead to turbulence in the stratified ocean interior are referred as internal processes, occurring away from the boundaries and producing energy internally. The most common are breaking internal waves and double-diffusive convection.

Buoyancy and momentum fluxes in the ocean lead to three main types of boundary layer turbulence:

(a) The stress is negligible where turbulence is exclusively generated by buoyancy fluxes from unstable stratification and convection. In such case, the dissipation of TKE is equal to the buoyancy flux;

(b) There is no buoyancy flux and the turbulent motion is driven by the wind stress or bottom friction on the boundary layer. In this situation, dissipation of TKE balances the shear production;

(c) There is both stress and buoyancy flux.

The ocean is rarely, probably never, in either the states represented in types (a) and (b), being (c) the regular state of the ocean boundaries.
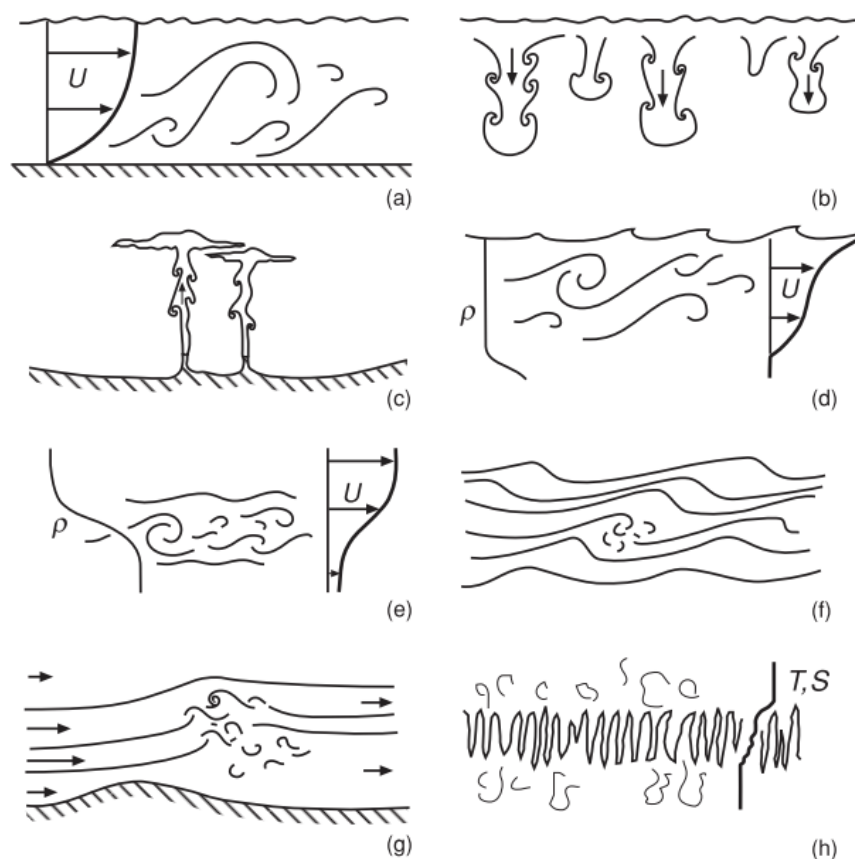
Fig. 1.2: Mixing processes according to their source of energy. (a) Turbulence produced by tidal or wave-induced flow over a solid boundary. (b) Convection resulting from surface cooling. (c) Mixing in an plume from a hydrothermal vent. (d) Turbulence due to wind-driven shear. (e) Mixing due to shear flow at the base of the surface layer. (f) Mixing from breaking internal waves. (g) Hydraulic jump. (h) Double-diffusive mixing. From Thorpe (2007).

1.2.1.1   Convection

Cooling at the sea surface creates parcels of cool, dense fluid, which sinks to a depth determined by the local stratification in a process known as convection (Fig. 1.2, (b)). Cooling occurs almost every night and sometimes at daytime due to weather systems that transport cold air masses. Convection may also be caused by an excess of evaporation over precipitation, which increases salinity, hence density, at the surface. Winds can aid convection by stirring the sea surface, thereby disrupting the viscous sublayer and permitting a more rapid transfer of heat and salt through the surface. Surface tension and viscous forces initially prevent denser surface fluid parcels from sinking. Once the fluid becomes sufficiently dense, however, those forces are overwhelmed and fluid parcels sink in the form of convective plumes. The relative motion of the plumes can generate small-scale turbulence, resulting in a turbulent field with scales spanned from the depth of the surface mixed layer (hereafter SML) to a few millimeters, the order of magnitude of diffusive processes (Gargett, 2003).When the wind stress is negligible, surface mixing is dominated by convection and there is a balance between ϵ and the buoyancy flux, B_f, as the rate of consumption of TKE by the upward B_f is similar to the rate dissipation (Shay and Gregg, 1986).

1.2.1.2   Wind stress

Wind stress over the ocean surface is possibly the main source of turbulence in the surface layer, not only because it induces instability by velocity shear, but also by the generation of oscillations that transfer momentum and energy from the atmosphere into the ocean. The surface wind stress can be expressed by

$$\tau_{wind} = \rho_{air} C_D W_{10}^2,$$ (1.6)

where ρ_{air} is the density of air, C_D the drag coefficient and W_{10} is the wind speed at 1 atm (i.e., 10 m above sea level). Wind stress at the surface generates a sheared velocity profile (Fig. 1.2, (d)) that induces vertical mixing due to eddies yielded by small scales oscillations on the vertical velocity field. The wind shear is highly effective in producing vertical mixing, as it can increase the depth of the SML considerably, as well as to mix the entire water column at shallow waters when added to the bottom stress. In addition, mixing by wind-driven shear is more effective than the one yielded by convection. The depth of influence of the wind stress is determined by

$$D = \pi \sqrt{\frac{2\nu_e}{f}},$$ (1.7)

where ν_e is a eddy viscosity coefficient and f the Coriolis parameter. The depth D is a length scale called the Ekman depth, which is an indicator of the depth to which the

influence of the surface stress penetrates the water column. In general, D coincides with the SML depth. Due to Earth's rotation effects, wind-driven currents often steer with depth, generating the Ekman transport, a net barotropic flow 90 degrees to the right (in the northern hemisphere) of the wind direction.

The rapid diffusion of momentum induced by the wind stress through the mixed layer may concentrate shear at the SML base, increasing the probability of occurrence of small-scale instabilities and generation of shear induced mixing (Fig. 1.2, (e)). Some of the energy released by the instabilities propagates along the stratified layer as internal waves, at larger spatial scales, or can lead to diffusive mixing, at smaller scales.

The transfer of momentum due to wind stress generate different oscillatory motions at the surface and the breaking of those oscillations leads to dissipation of energy and thus turbulence generation. Examples of surface wind-driven oscillations are the surface gravity waves, whitecappings (Simpson and Sharples, 2012), inertial waves (Simpson et al., 2002) and the Langmuir circulation (McWilliams et al., 1997). Some of these processes are sketched in Fig. 1.3.
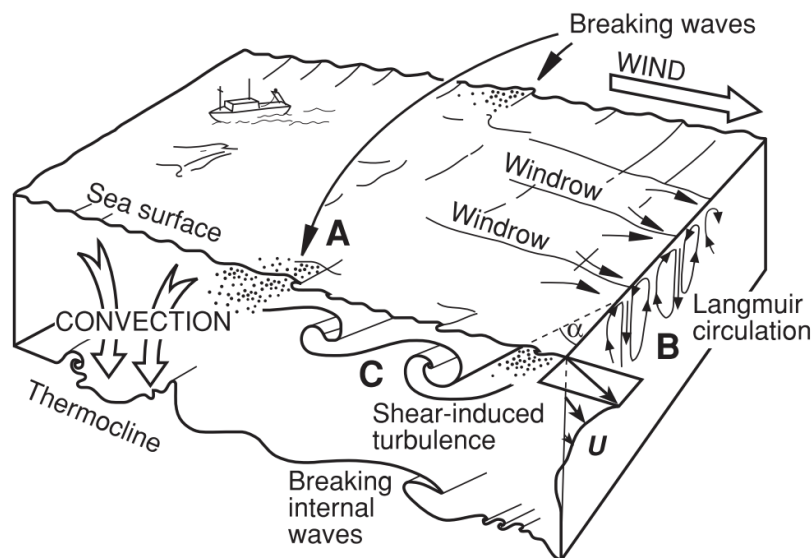
Fig. 1.3: A schematic ilustration of the processes leading to the mixing on the surface ocean boundary layer. **A** is breaking surface waves, **B** is the Langmuir circulation and **C** is the shear-induced turbulence. Convection and internal wave breaking are sketched as well. From Thorpe (2007).

1.2.1.3   Bottom boundary layer

The presence of a physical static boundary, as it happens at the bottom of the ocean, modifies the turbulence in the vicinity. Near the virtually immobile seabed, viscous forces tend to reduce the components of velocity parallel to the boundary (i.e., tangential components) to zero (or almost zero when the bed material is mobile). The physical boundary constrains and modifies the form and scale of turbulence by sup-

pressing the normal components flux velocity in its vicinity. At the sea surface, normal components are lost in breaking waves or other processes that cause fluid to be carried through the surface, or from the boundary layer into the underlying water column. Flow separation or subduction processes are usually observed in motions that are not confined to a static boundary. Flow separation, however, may occur as it does at the sea surface when, for example, water moves over the crests of ripples on a mobile seabed, sometimes carrying sediment particles from the bottom into suspension.

The stress produced by the seabed over near-bottom flows is expressed by $\tau_{bottom} = \rho_0 C_D U^2$, where U is the flow speed just above the seabed, which is analogue to the wind surface stress. The near seabed flow will generally be strongly affected by the sea floor or topographic roughness (e.g., Decloedt and Luther, 2010). The wake from the bottom components, from small rocks to steep seamounts, will determine the spatial and temporal variability of the flow near the seabed. Relatively large roughness can result in flow separation and the generation of small to mesoscale eddies, which are dependent to the physical size of the roughness component. Most of the energy dissipated at the bottom boundary layer comes from the flow produced by the mean circulation and by flows induced by subsurface mesoscale eddies and internal waves. This energy input maintains a 5 to 60 m thick mixed benthic boundary layer. At flat bottoms, only small fraction of the energy may be made available for mixing well above the benthic boundary layer (e.g., Kunze and Sanford, 1996). Where the bottom topography intersects isopycnal surfaces, however, such as the continental slopes or regions with abrupt topography, turbulence in the boundary layer will result in enhanced mixing across density surfaces (i.e., diapycnal mixing), thus possibly affecting the levels way above seafloor (e.g., Kunze et al., 2006; Klymak et al., 2006). The enhanced mixing is observed to persist even up to several of meters above the topography.

Another source for bottom mixing is one particular case of convection in the ocean that occurs as a result of the release of very hot and buoyant fluid from hydrothermal vents (Fig. 1.2, (c)). Hydrothermal vents are found in the ocean floor in the vicinity of oceanic ridges, producing rising plumes of water that is much less dense than its surroundings. The rising hot-fluid plume generates perturbations in the surroundings, leading to local turbulent mixing.

1.2.2 Turbulence in the stratified ocean interior

Mixing processes in the stratified interfaces of the ocean derive their energy internally from sources that may or may not be driven by external forcing at the boundaries. Two processes usually dominate the generation of turbulence and diapycnal mixing in the stably stratified ocean. The first is instability resulting from the motion of shear-stratified flows. Denser water moved upwards into less dense water in the stratified

ocean is subjected to a net downward force, whereas an upward force is experienced by water moved downward. These forces lead to oscillatory motions or waves, called internal waves. The second process is more subtle, occurring in the form of a small-scale convection that results from the different molecular diffusion coefficients of heat and salt, called double-diffusive convection (hereafter DDC). While internal waves and DDC convection are ubiquitous features in the ocean, turbulence may also occur at the interfaces between river or estuarine plumes and oceanic waters. The presence of river plumes have a direct influence on the turbulence pattern in coastal regions.

1.2.2.1 Internal waves

Internal gravity waves, or simply internal waves, occur in density-stratified fluids because of gravitational restoring forces acting on vertically displaced fluid. They can be generated by atmospheric forcing and/or interactions with the topography, and propagate long distances in the ocean. Similar to surface gravity waves, internal waves travel horizontally along isopycnals, but in continuous stratification internal waves can propagate at an angle to the horizontal, transporting energy in a vertical direction across isopycnals in wave beams (rather than becoming surface trapped as surface waves). Thus, internal waves have both horizontal and vertical wavenumber. Their upward and downward propagation through the stratified ocean provides a means of energy transport to the seabed and the sea surface, but adds complexity to the problem of predicting the distribution, persistence and the nature of mixing caused by their breaking.

The nature of internal waves motion is akin to the motion at stratified rotating fluids, e.g., the ocean. In the continuously stratified ocean internal waves can propagate an any direction and at any angle to the vertical. The dispersion is isotropic for k and l, the horizontal wavenumbers in the x and y directions, respectively, but anisotropic for m, the vertical wavenumber component. The dispersion relation of internal waves may be obtained from the equations of motion. After a a series of mathematical steps, as showed in Kundu et al. (2001), the velocity field of internal waves is

$$
\begin{aligned}
u &= \pm \frac{A(z)m}{k} cos(kx \pm \phi - \omega t), \\
v &= \pm \frac{A(z)mf}{\omega k} sin(kx \pm \phi - \omega t), \\
w &= A(z)\, cos(kx \pm \phi - \omega t).
\end{aligned}
\tag{1.8}
$$

The wave amplitude is $A(z) = A_0/\sqrt{m(z)}$, where A_0 is a constant value, and the wave phase is $\phi = \int^z m\, dz$, with the lower limit of the integral being arbitrary. As f only varies with y, it only appears in the v equation.

An equation for the vertical wavenumber m can be obtained by rearranging the

equations of motion and obtaining a single equation for w. The resulting expression is

$$m(z)^2 = \frac{k^2(N(z)^2 - \omega^2)}{(\omega^2 - f^2)}, \tag{1.9}$$

where $m(z)$ is the depth dependent vertical wavenumber. The relation shows that the dispersion of internal waves is controlled by the local stratification and the Earth's rotation, and internal waves only occur within the frequency range of

$$f < \omega < N, \tag{1.10}$$

assuming $N > f$, which is true for most of the ocean.

The frequency of oscillation of internal waves must be less than the maximum local stratification, which provides an upper limit to the local frequency of internal wave oscillations, as well as to discriminate between waves and turbulence. Hence, fluctuations with frequencies greater than N_{max} cannot be internal waves and are usually associated with turbulence (Gregg, 1989). While the range $f < \omega < N$ is a coherent threshold to classify internal waves oscillations, there is no clear physical distinction between internal waves and turbulent motion. Internal waves generate turbulence when breaking (Fig. 1.2, (f) and Fig. 1.3), and turbulence may generate oscillations that radiate from a turbulent subsurface patch along isopycnals. These induced oscillations may remain periodic with wave-like characteristics.

If one rearranges (1.9) as

$$\frac{m^2}{k^2} = \frac{(\omega^2 - f^2)}{(N^2 - \omega^2)}, \tag{1.11}$$

the ratio m^2/k^2 can be defined as the internal wave characteristic slope, as $tan\theta = m/k$, where θ is the angle between the direction of the wavenumber vector **K** with the horizontal. θ is thereby a function of f, N and ω. Hence, the internal wave angular frequency depends only on the direction of the wavenumber vector and not on its magnitude, which is different from surface gravity waves. Another contrasting feature between internal and surface waves is that internal waves have phase and group velocity vectors perpendicular to each other. Phase velocity c is along the axis of K, perpendicular to the crests. The group velocity c_g is parallel to the crests, meaning that internal waves transport energy orthogonally to its main path of propagation. A schematic of the geometric parameters for internal waves is shown in Fig. 1.4.

As internal waves provide means of transfer kinetic energy within different levels within the ocean, they are mostly important in costal regions, specially of abrupt topographic changes (Lamb, 2014; Sarkar and Scotti, 2017). A consequence of their dispersion along variable bathymetry is the breaking from reflecting, or being generated at, critical slopes. As described earlier, internal waves can travel with an angle θ
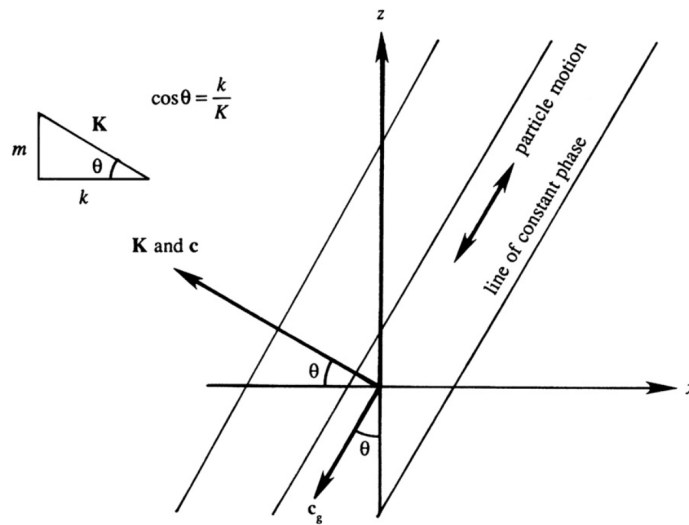
Fig. 1.4: Geometric parameters for internal waves. In this sketch from Kundu et al. (2001), z is vertical and x is horizontal. The phase velocity c is along the axis of the wavenumber vector **K**, which is the direction of propagation of an internal wave. The group velocity, c_g, however, is orthogonal to c, meaning that internal waves transport energy along the axis of their crests. The ratio m/k, i.e., $tan\theta$, provides the internal wave characteristic slope with the horizontal, an important parameter in the turbulence generated by internal waves interacting with the topography.

with the horizontal, and the wave slope with regard the topography slope may cause different means of how internal waves interact with the bathymetry. Critical slopes are found where the ratio between the wave slope, estimated from ω, f and N, and the topographic slope, the spatial gradient of the bathymetry, are close to unity. Thus, the behavior of normally incident internal waves approaching the topography can be predicted from this relatively simple ratio, namely α. When the ratio between slopes is less than unity, called a subcritical regime, internal waves will propagate with very little interaction with the topography. When α is larger than unity, waves will be partly reflected from the topography, which is called a supercritical regime. However, when $\alpha \approx 1$, the internal wave interacts with the topography, leading to , wave breaking, non-linear effects and, therefore, turbulence generation (Wunsch, 1968). Breaking of internal waves occurs as their angular frequency surpass the local stratification, leading to increased shear instabilities and generation of KH billows, allowing the vertical diffusion of several properties, such as heat and nutrients (Gargett and Holloway, 1984). Enhanced vertical shear, shoaling and bottom boundary layer instabilities as they reach and interact with critical or near critical slopes are mechanisms responsible for internal wave breaking (Lamb, 2014).

Another important motion related to internal waves, mainly observed in sites of complex bathymetry, is internal tides. The vertical oscillations of the ocean surface is mainly linked to the barotropic tidal flow. The barotropic tidal currents have a nearly constant velocity profile, apart from near the seabed, where velocities are reduced due to bottom friction. At very shallow flat bottoms, barotropic tidal flows can produce

a sheared velocity profile that will generate significant turbulent mixing through verti-
cal instabilities (Fig. 1.2, (a)). In the deep ocean, however, barotropic tidal velocities
are generally very weak, of order 0.1 ms^{-1}, and dissipation is generally very small.
But when weak deep-ocean barotropic flow encounters steep topography with critical
slopes, the interaction induces a non-linear response and increased baroclinic veloc-
ities (Garrett and Kunze, 2007; Legg, 2016), which result from the transfer of energy
from the barotropic to the baroclinic flow. This barotropic to baroclinic transition en-
hances the local levels of turbulence (e.g., Egbert and Ray, 2000) and can generate a
baroclinic tide, or internal tide, that oscillates at the same frequency of the strongest
local tidal component (Garrett and Kunze, 2007). These internal tides travel within spe-
cific isopycnals levels, yielding patches of turbulent mixing along the wave beam (e.g.,
Lueck and Mudge, 1997; Lien and Gregg, 2001; Carter et al., 2006). Internal tides can
travel large distances before completely breaking into turbulence.

The flow of barotropic tidal currents across shelf-breaks or over small topographic
features (generally with $\mathcal{O}(10^3)$ m or less) can also generate hydraulic jumps (Fig. 1.2,
(g)). Hydraulic jumps occurs when a supercritical flow changes to subcritical[6], releasing
mechanical energy to conserve momentum. This released energy is usually dissipated
locally by turbulence (e.g., Nash and Moum, 2001). Hydraulic jumps have also shorter
wavelengths than internal tides.

Although turbulence produced by internal wave shear is an intermittent process
found in ~5-10% of the stratified ocean interior, they constitute one of the most impor-
tant processes of mixing in the stratified ocean (Kunze, 2003). While their dynamics is
generally complex, the understanding of the underlying mechanisms of internal wave
motion is necessary to evaluate the implications of their breaking. The enhanced sub-
surface mixing generated by internal wave breaking have direct consequences on the
distribution of properties, such as nutrients, which in turn have implications of local
rates of biological productivity, specially in regions of complex topography.

1.2.2.2   Double-diffusive convection

While internal wave breaking contributes substantially to the mixing of the stratified
ocean, double-diffusive convection (hereafter, DDC) occurs at interfaces with weak to
moderate stratification in which the vertical gradients of temperature and salinity have
the same sign. Mixing by convection due to diffusion of heat and salt appears as
vertical filaments across the density interface (Fig. 1.2, (h)) and is only observable with
microstructure measurements, as it occurs in the spatial scale of diffusive processes,

---

[6]The threshold between a supercritical and subcritical flow is given by the Froude number, $Fr = U(gH)^{-1/2}$. Fr is the speed-length ratio, a dimensionless number defined as the ratio of the flow inertia to the external field. Supercritical flows have $Fr > 1$ and dominated with kinetic energy. Conversely, subcritical are dominated by potential energy.

i.e., $\mathcal{O}\left(10^{-2}\right)$ to $\mathcal{O}\left(10^{-3}\right)$ m. In addition, the dynamics of DDC is much slower when compared to the mixing generated by internal waves.

The initial signature of instability in a DDC regime is a spatially coherent structure containing layers of uniform temperature and salinity. The layers appear as a staircase like structure in the temperature and salinity profiles, stacked one above the other with a variable size range, from centimeters to meters (Fig. 1.5). The layers are sustained by a convective small-scale B_f through the stratified layer.

The DDC regime can occur due to two types of vertical distributions of temperature-salinity (TS) profiles:

(a) Salt-finger regime (SFR): When less dense but warmer and saltier water lies over colder fresher water, DDC is developed in the form of salt-fingers. Because the molecular diffusivity of salt is very much less than one of heat (typically two to three orders of magnitude) (Stern, 1960), the density of the relatively cold and fresh layer beneath becomes less due to heat transfer from the top layer. The top layer increases density due to heat loss, and descending parcels of salt, in the form of fingers, are transferred vertically to the bottom layer, triggering small-scale instabilities and possible mixing.

(b) Diffusive regime (DR): When relatively colder and fresher water is displaced downward into a warm and salty water layer underneath, the colder water becomes less dense as a consequence of heat transfer with its relatively warm but salty surroundings. The now less dens water rises due to positive buoyancy to recover its original position, but having achieved a lower density than when it started, surpasses its original position and continues to rise, but now losing heat and becoming denser. The subsequent sinking and rising lead to a growing oscillation along the stratified interface between layers. The magnitude of the oscillation may lead to a convective heat, that in turn lead to small-scale mixing (Kelley et al., 2003).

A parameter that expresses the nature of double-diffusive instability is the density gradient ratio

$$R_\rho = \frac{(\alpha dT/dz)}{(\beta dS/dz)}, \tag{1.12}$$

where α the thermal expansion rate and β is the haline contraction rate. $\alpha dT/dz$ is the contribution of the mean vertical temperature gradient to the vertical density gradient and $\beta dS/dz$ is the corresponding contribution of the mean vertical salinity gradient.

If salinity increases and temperature decreases with depth, both contributions lead to increase density with depth and yield a negative density gradient. This is a regime of static stability defined as doubly stable. In the opposite case, both contribute to
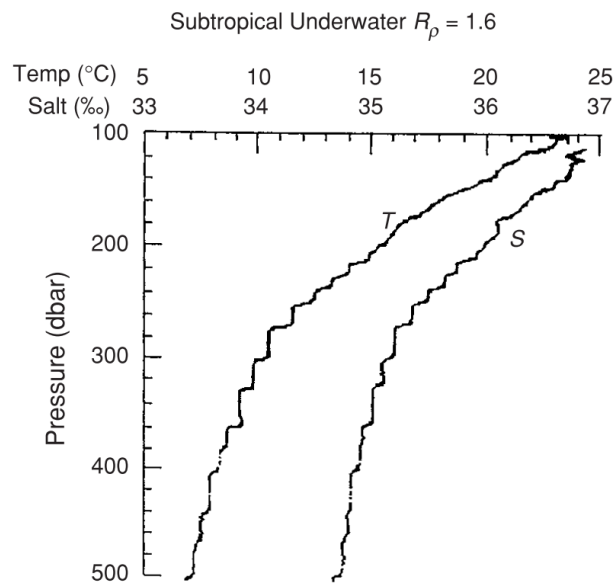
Fig. 1.5: Thermohaline staircase at depths between 200 and 400 m measurements obtained by Schmitt (1981) in the subtropics. As both TS diminish with depth, it is a SFR favorable profile, with R_ρ = 1.6. From Thorpe (2007).

a density that decreases with depth. Consequently, the density gradient is positive and the water column is statically unstable. R_ρ is less than zero in the doubly stable and in the statically unstable regime, but greater than zero when DDC is prone to be developed. DR occurs within the range $0 < R_\rho < 1$, because both dT/dz and dS/dz must be negative (increasing with depth). SFR occurs when $R_\rho > 1$, as dT/dz and dS/dz shall be positive (decreasing with depth).

Overall, the diapycnal mixing of heat and salt by diffusion only, i.e., in the lack of shear, is very small when compared to the isopycnal transport (e.g., Ledwell et al., 1993), as the vertical gradients are much larger than the horizontal gradients (Souza et al., 1997). The presence of shear is crucial to facilitate the transport across isopycnals. However, the development of salt-finger diffusivity is usually inhibited by shear (Kunze, 1994), being more effective at low to moderate shear-stratified interfaces. The diffusion of heat, on the other hand, may not be affected by shear (Padman, 1994).

The SFR may occur within the range $1 < R_\rho < 100$ (Schmitt, 1979). However, in an ocean constantly perturbed by internal waves, instabilities with frequency much lower than the local buoyancy frequency may not be developed (St. Laurent and Schmitt, 1999). Schmitt and Evans (1978) suggested that only instabilities that oscillate close to the local N will become established, what occurs when $1 < R_\rho < 2$, i.e., when stratification is too strong, SFR will fail to occur.

In the SFR, when the shear input is weak, i.e., $Ri_g > 0.25$ and there is moderate stability, DDC may contribute significantly to the mixing process, even when in thermohaline staircases are not developed (e.g., Thorpe, 2007). The convection driven

by salt and heat diffusion does not involve turbulence, as the motions are mostly laminar. It may lead, however, to weak the local level of stratification and facilitate the action of the shear turbulence. The SFR is the best indicator of DDC and the most used in oceanographic studies (e.g., Schmitt, 1981; St. Laurent and Schmitt, 1999; Fernández-Castro et al., 2014). Salt-fingers are well developed small scales structures that only occur within a particular range of shear and stratification (Kunze, 2003), generally constrained in a narrow range of R_ρ and Ri_g (e.g., St. Laurent and Schmitt, 1999).

Double-diffusive processes transport heat and salt occur at different rates, as a direct consequence of the large ratio between molecular diffusivity of heat and salt, being $D_T/D_S \approx 100$ (Gargett, 2003). Laboratory (Turner, 1968) and numerical studies (Merryfield et al., 1998) indicate that heat is transported more effectively than salt in shear induced turbulence. However, turbulent transports of heat and salt in the ocean are significantly different than the ones observed in laboratory, since the high Reynolds number oceanic turbulence may reduce considerably the magnitude of diffusive processes (Gargett, 2003).

1.2.2.3   Turbulence in river/estuarine plumes

River/estuarine plumes are flow structures which result from the discharge of rivers and estuaries into the adjacent ocean. Freshwater plumes occur in a large range of sizes and shapes, and their structure is primarily determined by the river/estuary freshwater outflow. Depending on their magnitude, freshwater plumes may have a major influence on the dynamics, water properties and circulation patterns of coastal regions (e.g., Peters, 1997; Hetland, 2005; MacDonald et al., 2007). Regions affected by river plumes are referred to as regions of freshwater influence (ROFI) (Simpson, 1997). Although the freshwater discharge is the most important parameter (and possibly the most variable) in the structure of a plume, tidal amplitude, coastline shape, local bathymetry, ambient ocean currents and wind stress can also affect their dynamics. Moreover, large-scale plumes whose horizontal length surpass the local Rossby radius of deformation, are also affected by Earth's rotation.

Mixing in freshwater plumes occurs through dyapicnal transport of buoyancy and momentum at the plume interface (Ivey et al., 2008), as the presence of a plume in the ocean forms a two-layer fluid system with different densities and properties. Therefore, quantification of mixing is given by the turbulent transport of momentum and buoyancy fluxes (Horner-Devine et al., 2015). The diapycnal mixing is primarily driven by KH instabilities, although their development depends on the level of stratification and the strength of the plume's advection, which in turn is driven by its buoyancy and wind shear. Usually, buoyant plumes have a small aspect ratio (low depth compared to horizontal distance) and thus vertical mixing is generally considered to be dominant
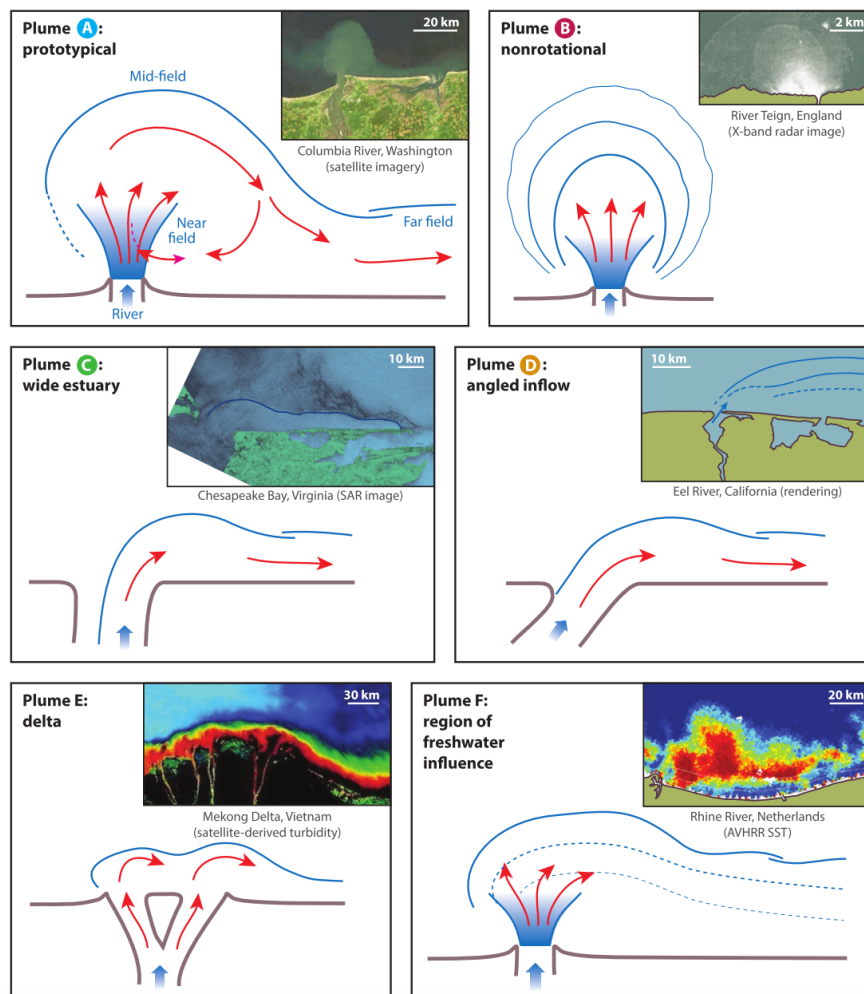
Fig. 1.6: Plumes shapes based on the advection outside their respective river/estuarine system. (a) Prototypical, (b) non-rotational, (c) wide estuary, (b) angled inflow, (e) delta plume and (f) region of freshwater influence. From Horner-Devine et al. (2015)

over the horizontal turbulent fluxes.

As freshwaters plumes occur in a vast range of sizes and shapes, it is hard to establish a constant turbulent mixing pattern. Fig. 1.6, from Horner-Devine et al. (2015), shows a summary of plume shapes and their respective river/estuarine systems. The prototypical type, appears to have the most complex turbulence mixing pattern, as they have three distinct regions in terms of mixing: the near, mid and far-field regions. In this type of plume, circulation is forced by a narrow channel and the Coriolis force. Some of the most intense mixing occurs in the near-field region (e.g., MacDonald et al., 2013), the jet-like region of initial expansion where the momentum of the plume surface layer dominates over its buoyancy, creating a strong vertical shear that results in intense mixing. Between the near and far-field, the mid-field region is where the Earth's rotation begins to dominate, restraining the plume offshore spreading and turning it to the right (in the northern hemisphere) of the estuary/river mouth. A stratified-shear flow may occur due to deceleration in the mid-field, increasing frontal mixing. Large-scale

plumes such as the La Plata and Chesapeake Bay estuaries plumes, however, do not present a near and mid-field regions, and the most intense mixing is expected to be found away from the source, the far-field region. This region is where the plume no longer has a memory of the initial momentum of the river discharge and the dynamics is primarily governed by Earth's rotation and wind stress, although buoyancy and bottom stress can still affect it.

Wind shear may be an important factor on generating mixing at river plumes, although previous studies showed lower turbulence levels than are observed in more energetic areas such as the near-field (e.g., Wang et al., 2015). Wind stress normally acts over the entire plume, but it is most effective in the far-field region due to weaker stratification. Mixing by wind occurs due to shear at the surface Ekman layer, but the wind influence is usually restricted to the freshwater surface layer (Lentz, 2004). The influence of wind on the far-field plume is modified by upwelling or downwelling winds, which tend to thin or thicken the plume, respectively, thus modifying the mixing response (Fong and Geyer, 2001). Intense turbulence may be observed in plume fronts in regions forced by strong tidal currents, but while turbulence is very high at the front, it decays exponentially behind the front, resulting in a narrow band of active mixing (e.g., O'Donnell et al., 2008). In shallow shelves with strong tides, bottom stress associated with the tidal flow may mix the plume from the bottom up (e.g., Simpson, 1997).

1.3 Turbulence quantification

The detailed structure of turbulent flows is rather unpredictable and, therefore, very difficult to measure. In spite of the challenges, the measure of turbulence is crucial to quantify the internal transports of mass, energy and momentum in the geophysical fluids dynamics. The quantification of turbulence is based on systematic sampling and averaging of the processes that lead to turbulence. A statistical description for stationary, homogeneous and isotropic turbulence has allowed the comprehension and description of turbulent flows in nature in terms of strain rates, spectra and probability density functions (Moum and Rippeth, 2009).

As the magnitude of turbulence of a given flow can be quantified by the rate of TKE dissipated by viscous forces into heat, the heat flux is one of the most important factors to describe the process of turbulent mixing. Besides the experiment of Osborne Reynolds with laminar and turbulent flows, another important experiment in the study of turbulence was the one by James Prescott Joule, published in the nineteenth century. Joule found the relation between changes of potential to kinetic energy and the temperature change resulting from the dissipation of that energy, a relation that is the base of turbulent motions. The essence of Joule's experiment is that falling weights lose potential energy in driving paddles within a cylinder filled with fluid (water and mercury),
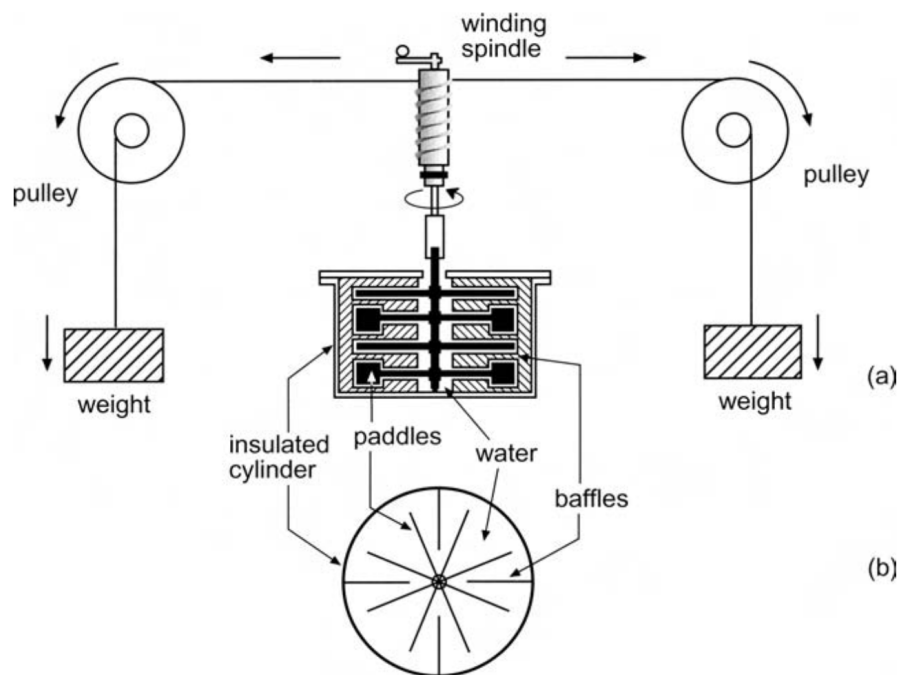
Fig. 1.7: A schematic representation of Joule's experiment. The cylinder is filled with a fluid, which is stirred with paddles driven by falling weights through the linkage pulley system. From Thorpe (2007).

leading to stir the fluid and heating it. The conclusion is that the lost of potential energy leads to gains in two different forms of energy: kinetic energy and heat. The key of his experiment is the baffles fixed to the inside of the cylinder. These accelerate the transfer of TKE from the mean flow to irregular small-scale eddies that enhance the shear within the fluid. Hence, this greatly increase the rate of dissipation of TKE through molecular viscosity and transfer mechanical energy into heat much more rapidly than would occur only by drag at the cylinder walls[7]. The potential energy of the falling weights that is not transferred to their kinetic energy, i.e., not used to stir the fluid, consequently passes into turbulent energy that is dissipated into heat. Therefore, Joule's experiment shows that turbulence transfers the energy of motion, i.e., the TKE, to heat. A schematic representation of the experiment is shown in Fig. 1.7.

1.3.1 The energy balance

As described in section 1.2, the energy for oceanic turbulence comes from a variety of sources and, as any natural system, in order to maintain the equilibrium, the rate of turbulent energy produced shall be in balance to its consumption and lost. The turbulent energy balance equation expresses the rate of changes in the total kinetic energy over time as a function of the rate of TKE production by the mean flow, i.e., the energy available from perturbations over the mean flow, the rate of transfer from kinetic

---

[7]The baffles inside the cylinder in Joule's experiment highlights the importance of the presence of obstacles (such as complex topography) on accelerate the transfer of energy from the mean flow and conversion into turbulence.

to potential energy (or vice-versa) and the rate at which kinetic energy is converted into heat through molecular viscosity.

Considering those three terms as dominant among the contributions to the rate of change of the mean kinetic energy of a turbulent flow, the balance equation can be expressed as

$$dE/dt = S + B - \epsilon, \tag{1.13}$$

where S is the TKE production from the mean flow, B is the buoyancy production and ϵ is the rate of dissipation of TKE. Assuming a steady state, the TKE does not change. Thus, $dE/dt = 0$ and the equation becomes

$$S + B - \epsilon = 0. \tag{1.14}$$

The TKE production, S, is the rate at which turbulent kinetic energy is produced by the mean flow, being the rate of work of the Reynolds stress, τ, that is exerted by the turbulent motion on a mean shear flow, dU/dz. The TKE production is also the rate of kinetic energy transferred from the mean flow to the turbulent flow.

The buoyancy production, B, is equal to the rate at which the turbulent motions increase the potential energy of the fluid or the rate at which turbulent motions are provided with kinetic energy as a result of a loss of potential energy. If B is negative, the buoyancy flux, B_f, is consuming kinetic energy to gain potential energy to work against gravity. B_f removes TKE from the mean flow to yield mixing, as it gains potential energy when moving fluid upwards. In a situation where $S \approx 0$ (e.g., convection in the absence of wind shear) B_f becomes the only possible source for TKE production and dissipation, and hence $-B = \epsilon$. Alternatively, if B is positive, the fluid is losing potential energy and buoyancy flux is providing kinetic energy to the energy balance. This occurs, for example, when a water column is being stratified. During stratification, B loses potential energy (since no energy is required to stratify) and kinetic energy becomes available.

The energy balance is an analytical description of Joule'e experiment, as the TKE removed from the mean flow can either be consumed for mixing in the potential energy gain, or be dissipated as heat.

1.3.2 Theoretical description of turbulence

In order to obtain a theoretical description of turbulence, the perturbations over the mean flow, neglected in the large-scale circulation, must be considered, as well as the

terms of viscous friction. It begins with the Navier-Stokes equations

$$\vec{\nabla} \bullet \vec{V} = 0,$$

$$\frac{\partial u}{\partial t} + \vec{V} \bullet \vec{\nabla} u = -\frac{1}{\rho_0} \frac{\partial P}{\partial x} + \nu \nabla^2 u,$$

$$\frac{\partial v}{\partial t} + \vec{V} \bullet \vec{\nabla} v = -\frac{1}{\rho_0} \frac{\partial P}{\partial z} + \nu \vec{\nabla}^2 v, \tag{1.15}$$

$$\frac{\partial w}{\partial t} + \vec{V} \bullet \vec{\nabla} w = -\frac{1}{\rho_0} \frac{\partial P}{\partial z} - \frac{g}{\rho_0}(\rho - \rho_0) + \nu \nabla^2 w,$$

where ν is the kinematic viscosity and $\vec{V} = u\vec{i} + v\vec{j} + w\vec{k}$. The Coriolis term is negligible at small scales, since it only affects large-scale motions. The variables on (1.15) represent their respective instantaneous quantities. If the flow is considered to be stationary, the Reynolds decomposition[8] can be applied over velocity, pressure and density, being

$$u = \overline{u} + u',$$

$$v = \overline{v} + u',$$

$$w = \overline{w} + u', \tag{1.16}$$

$$P = \overline{P} + P',$$

$$\rho = \overline{\rho} + \rho'.$$

To obtain the mean momentum equations, the decomposed terms in (1.16) are added into (1.15) and the spatial average is computed, which gives

$$\overline{\frac{\partial(\overline{u} + u')}{\partial t}} + \overline{(\vec{V} + \vec{V'}) \bullet \vec{\nabla}(\overline{u} + u')} = -\frac{1}{\rho_0} \overline{\frac{\partial(\overline{P} + P')}{\partial x}} + \nu \overline{\nabla^2(\overline{u} + u')},$$

$$\overline{\frac{\partial(\overline{v} + v')}{\partial t}} + \overline{(\vec{V} + \vec{V'}) \bullet \vec{\nabla}(\overline{v} + v')} = -\frac{1}{\rho_0} \overline{\frac{\partial(\overline{P} + P')}{\partial y}} + \nu \overline{\nabla^2(\overline{v} + v')}, \tag{1.17}$$

$$\overline{\frac{\partial(\overline{w} + w')}{\partial t}} + \overline{(\vec{V} + \vec{V'}) \bullet \vec{\nabla}(\overline{w} + w')} = -\frac{1}{\rho_0} \overline{\frac{\partial(\overline{P} + P')}{\partial z}} - \frac{g}{\rho_0}\overline{(\overline{\rho} + \rho' - \rho_0)} + \nu \overline{\nabla^2(\overline{w} + w')}.$$

Spatial averages of the mean quantities are equal to their own averages and the spatial

---

[8]In fluid dynamics and turbulence theory, Reynolds decomposition is a mathematical technique used to separate the quantity into the sum of its respective mean and the zero-mean fluctuations. The objective is to obtain an approximate time-averaged solutions for each quantity.

averages of the fluctuations are zero, which results in

$$\frac{\partial \overline{u}}{\partial t} + \overrightarrow{\overline{V}} \bullet \vec{\nabla}\overline{u} + \overline{\overrightarrow{V'} \bullet \vec{\nabla}u'} = -\frac{1}{\rho_0}\frac{\partial \overline{P}}{\partial x} + \nu\nabla^2\overline{u},$$

$$\frac{\partial \overline{v}}{\partial t} + \overrightarrow{\overline{V}} \bullet \vec{\nabla}\overline{v} + \overline{\overrightarrow{V'} \bullet \vec{\nabla}v'} = -\frac{1}{\rho_0}\frac{\partial \overline{P}}{\partial y} + \nu\nabla^2\overline{v}, \qquad (1.18)$$

$$\frac{\partial \overline{w}}{\partial t} + \overrightarrow{\overline{V}} \bullet \vec{\nabla}\overline{w} + \overline{\overrightarrow{V'} \bullet \vec{\nabla}w'} = -\frac{1}{\rho_0}\frac{\partial \overline{P}}{\partial z} - \frac{g}{\rho_0}(\overline{\rho} - \rho_0) + \nu\nabla^2\overline{w}.$$

Terms with the average of the product of the fluctuations, $\overline{u'\nabla\vec{V'}}$, $\overline{v'\nabla\vec{V'}}$ and $\overline{w'\nabla\vec{V'}}$, refer to the non-linear processes akin to turbulence produced by the tangential stress being exerted over the mean flow, i.e., the Reynolds stress. The stress terms, which result from the Reynolds decomposition, are expressed in the form of the Reynold tensors, $\tau_{i,j}$

$$\tau(\vec{V'}_i\vec{V'}_j) = \begin{bmatrix} \overline{u'u'} & \overline{v'u'} & \overline{w'u'} \\ \overline{u'v'} & \overline{v'v'} & \overline{w'v'} \\ \overline{w'u'} & \overline{w'v'} & \overline{w'w'} \end{bmatrix}. \qquad (1.19)$$

Turbulent motions can be interpreted as a ensemble of several eddies with different sizes and strengths, embedded within each other and changing intermittently, resulting in the random nature of turbulence. As the turbulent flow is assumed to be statistically steady in time ($dE/dt = 0$ in the energy balance), one can assume that the flow is spatially uniform and all eddies of a given size share the same characteristic velocity. Therefore, turbulence is considered to be stationary, homogeneous and isotropic (Cushman-Roisin and Beckers, 2011). As a consequence, the diagonal Reynold stress terms $u'u'$, $v'v'$ and $w'w'$ are equal, and the off-diagonal terms are zero. Therefore, the Reynolds tensors are reduced to

$$\tau(\vec{V'}_i\vec{V'}_j) = \overline{u'u'} = \overline{v'v'} = \overline{w'w'}. \qquad (1.20)$$

This assumption simplifies significantly the derivation of the equations for the kinetic energy of the mean and turbulent flows.

The equations that express the kinetic energy of the mean flow are obtained by multiplying (1.18) by the mean velocity field, $\overrightarrow{\overline{V}}$. The resulting output gives a scalar

quantity (i.e., mean kinetic energy), being

$$\frac{\partial(\frac{\overline{u}^2+\overline{v}^2+\overline{w}^2}{2})}{\partial t} + \overline{\vec{V}} \bullet \vec{\nabla}(\frac{\overline{u}^2 + \overline{v}^2 + \overline{w}^2}{2}) =$$

$$\vec{\nabla}\left[-\frac{1}{\rho_0}\overline{P\vec{V}} + \overline{(u'\vec{V'})}\overline{u} + \overline{(v'\vec{V'})}\overline{v} + \overline{(w'\vec{V'})}\overline{w} + \nu\vec{\nabla}(\frac{\overline{u}^2 + \overline{v}^2 + \overline{w}^2}{2})\right]+$$

$$[\overline{u'\vec{V'}} \bullet \vec{\nabla}\overline{u} + \overline{v'\vec{V'}} \bullet \vec{\nabla}\overline{v} + \overline{w'\vec{V'}} \bullet \vec{\nabla}\overline{w}]-$$

$$[\nu(\vec{\nabla}\overline{u} + \vec{\nabla}\overline{v} + \vec{\nabla}\overline{w})^2]-$$

$$\frac{g}{\rho_0}(\overline{\rho} - \rho_0)\overline{w} \tag{1.21}$$

The left-hand side (LHS) terms are the total derivative of the kinetic energy of the mean flow, $d/dt(\overline{\vec{V}}^2/2)$, and, as the energy is conserved, this term is zero (Kundu et al., 2001). The first term on the right-hand side (RHS) is the rate at which energy is added to the mean flow from internal forces, also called the redistribution term (Kundu et al., 2001). It represents the potential energy lost due to the pressure gradient, which is subject to Reynolds stress and the molecular friction. The second and third terms on the RHS are the losses due to Reynolds stress and molecular friction, respectively, exerted upon the mean flow (Kundu et al., 2001). Both work against it, transferring TKE to the turbulent flow. The last term is energy loss to gravitational potential energy by the mean vertical velocity, which is also negligible (Kundu et al., 2001).

To obtain the equations that describe the kinetic energy of the turbulent flow, more work is required. The mean momentum equations (1.18) must be subtracted from the Navier-Stokes equations for the total velocity (1.15) to obtain the equations for the velocity fluctuations field, $\vec{V'}$. The results is then multiplied by $\vec{V'}$ and averaged, which gives

$$\frac{d(\frac{\overline{u'^2+v'^2+w'^2}}{2})}{dt} =$$

$$-\vec{\nabla}\left[\frac{1}{\rho_0}\overline{P'\vec{V'}} + \frac{1}{2}\overline{(u'^2\vec{V'} + v'^2\vec{V'} + w'^2\vec{V'})} + \frac{\nu}{2}\vec{\nabla}\overline{(u' + v' + w')^2}\right]-$$

$$[\overline{u'\vec{V'}} \bullet \nabla\overline{u} + \overline{v'\vec{V'}} \bullet \vec{\nabla}\overline{v} + \overline{w'\vec{V'}} \bullet \vec{\nabla}\overline{w}]-$$

$$[\nu\overline{(\vec{\nabla}u' + \vec{\nabla}v' + \vec{\nabla}w')^2}]-$$

$$\frac{g}{\rho_0}\overline{\rho'w'}. \tag{1.22}$$

Similar to the mean flow, the term on the LHS (the total rate of change of the TKE), is zero. Also analog to the mean flow, the first term on the RHS is the redistribution of TKE, which is usually small because it is mainly dependent of fluctuations in the pressure field (Kundu et al., 2001). The last three terms on the RHS are the most

important, since they express analytically the energy balance. The second term on the RHS is the negative of the corresponding term in (1.21). It is the transfer of kinetic energy from the mean flow to the turbulent flow, i.e., the rate of production of TKE or shear production, S, being the main source of energy that sustains the turbulence (Kundu et al., 2001). The third term is the loss of kinetic energy, being the rate of dissipation of TKE by molecular friction into heat, the so-called ϵ, several orders of magnitude larger than the viscous term in the mean flow equation (Kundu et al., 2001). The gradients of velocity fluctuations can be very large in comparison to the very small spatial scales of the turbulent eddies. The last term is the loss or gain of TKE due to the vertical buoyancy flux, or also buoyancy production, B (Kundu et al., 2001). B, or B_f when referred as buoyancy flux, is a sink for TKE when transporting fluid mass upwards, leading to potential energy gain. Hence, $\rho' w'$ is positive. Alternatively, B_f is a source for TKE when moving mass downwards, i.e., loss of potential energy. Thus, $\rho' w'$ is negative. The analytical description of the TKE balance is thereby

$$S = -(\overline{u'\vec{V'}} \bullet \vec{\nabla}\overline{u} + \overline{v'\vec{V'}} \bullet \vec{\nabla}\overline{v} + \overline{w'\vec{V'}} \bullet \vec{\nabla}\overline{w}),$$
$$B = -\frac{g}{\rho_0}\overline{\rho'w'}, \tag{1.23}$$
$$\epsilon = \nu\overline{(\vec{\nabla}u' + \vec{\nabla}v' + \vec{\nabla}w')^2}.$$

The ϵ equation contains 9 terms, but in isotropic turbulence the dissipation can be expressed with a single component, for any given direction. Hence, the fluctuations can be reduced to

$$\overline{\vec{\nabla}u'} = \overline{\frac{\partial(u'^2)}{\partial x}} = \overline{\vec{\nabla}v'} = \overline{\frac{\partial(v'^2)}{\partial y}} = \overline{\vec{\nabla}w'} = \overline{\frac{\partial(w'^2)}{\partial z}}. \tag{1.24}$$

Therefore, the rate of dissipation of TKE for isotropic steady and homogeneous turbulence per unit of mass can be expressed by

$$\epsilon = \frac{15}{2}\nu\overline{\left(\frac{\partial u'}{\partial z}\right)^2}, \tag{1.25}$$

where $\partial u'/\partial z$ can be any of the 6 components of the shear variance.

By applying the Reynolds decomposition and averaging the equations of motion, equations that express how the viscous force affects the mean flow were obtained. This shows how small-scale processes act through the Reynolds stresses terms. However, as those terms are a function of the flow, they represent a new unknown to turbulence description. This adds to the closure problem of the ocean turbulence: it is not possible to resolve (analytically or numerically) the fluctuation terms from Reynolds decomposition (Cushman-Roisin and Beckers, 2011). The usual approach often used in global circulation models is to assume the stresses as an eddy viscosity coefficient, ν_e, which

gives

$$\overline{u'^2} = \nu_e \frac{\partial \overline{u}}{\partial x} = \overline{v'^2} = \nu_e \frac{\partial \overline{v}}{\partial y} = \overline{w'^2} = \nu_e \frac{\partial \overline{w}}{\partial z}. \qquad (1.26)$$

This approach states that the fluctuations can be parameterized into a constant that multiplies the spatial gradients of averages of the velocity field. This is based on the Boussinesq hypothesis for Reynolds stress (Boussinesq, 1877) and the Prandtl-Kolmogorov relationship (Moraes et al., 1998), which assume ν_e as an isotropic scalar quantity that can be related to the mean velocity gradients. This is an oversimplification used by models as it is not expected ν_e to be a constant, since it depends on characteristics of the flow, which are variable with time and space (Cushman-Roisin and Beckers, 2011). As the turbulence models rely on the parametrization of the fluctuations, observations obtained with microstructure profiles can provide the actual magnitude of the fluctuations to calibrate the models.

1.3.3 Temperature fluctuations variance

It is also possible to obtain equations that express the fluctuations variance of scalars (analogue to momentum), such as temperature and salinity[9]. As the fluctuations in the temperature field are a reliable proxy for turbulence and directly determined from thermistor data, only the equation for temperature variance will be showed here.

The equation of conservation of heat in the ocean is

$$\frac{\partial T}{\partial t} + \vec{V} \bullet \vec{\nabla} T = D_T \nabla^2 T, \qquad (1.27)$$

where D_T is the molecular thermal diffusivity. The temperature field can also decomposed into its mean field plus fluctuations, as in

$$T = \overline{T} + T'. \qquad (1.28)$$

Substitution of (1.28) into (1.27) and taking the average gives

$$\frac{\partial \overline{T}}{\partial t} + \overline{\vec{V}} \bullet \vec{\nabla}\overline{T} + \overline{\vec{V}' \bullet \vec{\nabla}T'} = D_T \nabla^2 \overline{T}. \qquad (1.29)$$

Subtracting (1.29) from (1.27) gives the equation for temperature fluctuations, T', which is

$$\frac{\partial T'}{\partial t} + \vec{V}' \bullet \vec{\nabla}\overline{T} + \vec{V}' \bullet \vec{\nabla}T' + \overline{\vec{V}} \bullet \vec{\nabla}T' - \overline{\vec{\nabla} \bullet \vec{V}'T'} = D_T \nabla^2 T'. \qquad (1.30)$$

---

[9]The salinity variance can be estimated from fluctuations in conductivity, but its interpretation may be limited by the fact that conductivity is dependent of both temperature and salinity. Thus, it is usually inferred from simultaneous measurements of conductivity and temperature from two separated sensors, which may lead to uncertainties in the estimated values (e.g., Nash and Moum, 1999)

Multiplying (1.30) by T' and taking the average results in

$$\frac{d\overline{T'^2}}{dt} + 2\overline{\vec{V}'T'\vec{\nabla}T} + \overline{\vec{\nabla} \bullet \vec{V}'T'^2} = D_T\vec{\nabla}^2\overline{T'^2} - 2D_T\overline{(\nabla T')^2}, \qquad (1.31)$$

and in a steady state $d\overline{T'^2}/dt = 0$.

In the conservation of temperature variance the most important terms are the turbulent heat flux down the gradient of mean temperature, $2\overline{\vec{V}T'\vec{\nabla}T}$ and square of the gradient of temperature fluctuations, $-2D_T\overline{(\vec{\nabla}T')^2}$. The turbulent heat flux is much larger than the molecular heat flux, $D_T\vec{\nabla}^2\overline{T'^2}$, and, in a steady state, is the only term that can produce temperature variance. The last term represents the rate of dissipation of temperature variance, or sometimes called the rate of loss of temperature variance [Thorpe (2007)], symbolized by χ_T

$$\chi_T = 2D_T\left[\overline{\left(\frac{\partial T'}{\partial x}\right)^2} + \overline{\left(\frac{\partial T'}{\partial y}\right)^2} + \overline{\left(\frac{\partial T'}{\partial z}\right)^2}\right], \qquad (1.32)$$

which at isotropic fluctuations becomes

$$\chi_T = 6D_T\overline{\left(\frac{\partial T'}{\partial z}\right)^2}, \qquad (1.33)$$

where $\partial T'/\partial z$, can be any of the 3 components of the temperature variance.

Momentum is transferred within fluids by inertial and pressure forces and by viscous friction, while heat and salt can only be transferred by molecular diffusion. Therefore, scalar fluctuations have smaller scales than those of velocity (Gibson and Schwarz, 1963). The scalar fluctuations are passive, occurring as a consequence of velocity turbulence field in the presence of a mean gradient of a scalar, such as pressure. Thus, scalar fluctuations, specially temperature, can be indicator of turbulence. When velocity variance is not available, one can explore this property to obtain an estimate of the turbulent field (e.g., Dillon, 1982).

1.3.4   Length scales

The description of the TKE flow shows that turbulence is a primarily a spatial phenomenon (Kundu et al., 2001). Its sources and sinks depend solely on the gradients of velocity, pressure and density (temperature and salinity), and, in a statistically steady state, temporal variations are often negligible[10]. Hence, the turbulence is characterized by length scales instead of time scales.

The scales of most of the motions in the ocean are derived by dimensional analysis

---

[10]For example, an eddy will advect past a position in a channel in a given time interval. For an observer at a fixed position, the velocity will appear to fluctuate rapidly. The eddy itself, however, remains statistically steady with constant fluctuations, i.e., no acceleration of the flow.

considering the forces that could significantly affect the motion. ϵ is a parameter that determines scales, since it adjusts itself to match the rate of energy production at the largest scales. The scale of the largest turbulent eddies[11] is the Ozmidov length scale

$$L_O = \left(\frac{\epsilon}{N^3}\right)^{1/2} [m].$$
(1.34)

L_O is restrained by the local buoyancy frequency when away from boundaries, and seldom exceeds 1 m. At spatial scales larger than L_O, the production of TKE is not enough to uphold turbulent mixing, i.e., to maintain the flow of kinetic energy into potential energy.

The scale at which viscous dissipation dampens out the velocity fluctuations and converts energy into heat is the Kolmogorov length scale

$$L_K = \left(\frac{\nu^3}{\epsilon}\right)^{1/4} [m].$$
(1.35)

At scales larger than L_K, the TKE will not be dissipated, as the magnitude of velocity fluctuations are very small compared to the mean flow. The scale of viscous dissipation depends on the fourth-root of ϵ and does not range widely, varying usually between $\mathcal{O}(10^{-7})$ and $\mathcal{O}(10^{-6})$ m. In the range $L_O \to L_K$ both buoyancy and viscous forces are unimportant and turbulence is mainly isotropic.

The scalar fluctuations are dampened by the molecular diffusion, which occurs in the Batchelor length scale

$$L_B = \left(\frac{\nu D_T^2}{\epsilon}\right)^{1/4} [m].$$
(1.36)

As L_B refers to spatial scales of molecular diffusion, it is smaller than L_K, of order $\mathcal{O}$ (10^{-3}) m. For salt diffusion, whose diffusivity is 2-3 orders of magnitude lower than heat, L_B can be significant small. Although other spatial scales can be used in the study of turbulence (e.g., Smyth and Moum, 2000; Mater et al., 2013), Ozmidov, Kolmogorov and Batchelor scales are the most commonly used scales.

1.3.5 Models of diffusivity

1.3.5.1 Osborn-Cox model for heat diffusivity

One of the first models for diapycnal mixing is the one from Osborn and Cox (1972), which assumes that turbulence is driven by vertical fluxes of heat. The vertical component is the main reference for background temperature and the flux of heat is solely vertical. In a steady and isotropic state, the production of temperature fluctuations is

---

[11]In this thesis, scales smaller than L_O are hereafter referred as micro-scales.

balanced by its rate of variance. Then, (1.31) can be written as

$$\overline{w'T'}\frac{\partial \overline{T}}{\partial z} = 3D_T\overline{\left(\frac{\partial T'}{\partial z}\right)^2}.$$ (1.37)

The eddy diffusion of heat, or the heat diffusivity, is defined as

$$K_T = \frac{\overline{w'T'}}{dT/dz}.$$ (1.38)

Isolating $\overline{w'T'}$ in (1.37) and (1.38) gives

$$\overline{w'T'} = K_T\frac{dT}{dz} = \frac{\chi_T/2}{\partial \overline{T}/\partial z}.$$ (1.39)

If in a steady state $dT/dz = \partial \overline{T}/\partial z$, (1.39) can be rearranged as

$$K_T = \frac{\chi_T}{2(\partial \overline{T}/\partial z)^2}.$$ (1.40)

Because χ_T provides a measure of the vertical flux of heat due to turbulence, scalar fluctuations allow the assessing the eddy diffusivity of an environment. It is, however an indirect estimate because momentum can be transferred by inertial and pressure forces at different rates than the molecular diffusion of temperature. The model relies on the passivity of scalars within the turbulent flow.

1.3.5.2 Osborn model for diapycnal diffusivity

The model from Osborn (1980) for diapycnal transport assumes a local balance among the TKE production, the buoyancy production and TKE dissipation. Once again, considering the turbulence as isotropic the S term in (1.23) can be simplified to

$$S = -\overline{u'w'}\frac{\partial \overline{u}}{\partial z}.$$ (1.41)

and all terms in the energy balance can rearrange as

$$\overline{u'w'}\frac{\partial \overline{u}}{\partial z} = \frac{g}{\rho_0}\overline{\rho'w'} - \epsilon.$$ (1.42)

Laboratory experiments indicate that the buoyancy production is $\sim$1/6 of the rate of TKE production (e.g., Ivey and Imberger, 1991). Substitution of this relation into the energy balance results in $B = \epsilon/5$. This 0.2 ratio is defined as the flux coefficient, symbolized by Γ. This quantity provides a measure of the efficiency of mixing, and older studies refer to Γ as indeed the mixing efficiency (e.g., Oakey, 1982). However, as pointed out by Moum (1996), Γ is in fact a constant of proportionality between the potential energy gain from upward transport, i.e., negative B_f, and the rate of TKE

dissipated. Therefore, Γ is the factor by which the dissipation rate must be multiplied to obtain the respective potential energy gain, being flux coefficient a more suitable designation (Smyth et al., 2001). The mixing efficiency is actually given by the flux Richardson number, R_f, defined as the ratio of buoyancy to shear production, $R_f = B/S$.

One can thereby conclude that this potential energy gain accounts for approximately 20% of the TKE dissipated by viscous friction, being the 0.2 value the most commonly used in turbulence studies. However, observational data suggests that Γ is, in fact, significantly variable (Moum, 1996; Gargett and Moum, 1995), evolving systematically in time as turbulent overturns grow, break, and decay (Smyth et al., 2001). A model for the spatial variability of Γ (which will be defined here as observed flux coefficient, Γ_{obs}) was proposed by Gargett and Moum (1995). When ϵ and χ_T are measured simultaneously, the flux coefficient is

$$\Gamma_{obs} = \frac{\chi_T N^2}{2\epsilon(\partial\overline{T}/\partial z)^2},$$ (1.43)

As Γ expresses the ratio of the diffusivities for heat and buoyancy to ϵ, in oceanic applications, when the flux coefficient exceeds the nominal value of 0.2 it means that DDC is mainly responsible for diapycnal mixing, rather than turbulence (Thorpe, 2007). $\Gamma > 0.2$ is commonly used as a threshold for to identify salt-finger mixing (e.g., St. Laurent and Schmitt, 1999; Fernández-Castro et al., 2014).

Based on Osborn's approach, a model for diapycnal diffusivity scaled by ϵ can be developed using the flux coefficient. If

$$\overline{\rho'w'} = -K_\rho\frac{\partial\rho}{\partial z}$$ (1.44)

and

$$B = \frac{g}{\rho_0}\overline{\rho'w'} = \Gamma\epsilon,$$ (1.45)

then

$$K_\rho = \frac{\Gamma\epsilon}{N^2}$$ (1.46)

This method is largely used to estimate diapycnal diffusivity in oceanic studies. The assumption is that the eddy diffusivities of heat, salt and density are equal or similar when the flux of scalars is driven by turbulence, which is what occurs for most of the ocean[12].

---

[12]Exception occurs when diffusive processes driven by DDC are more important than the ones due to shear, as it happens at high latitudes with large precipitation rates or in a freshwater lake (Schmitt, 1994), resulting in different rates of diffusivity of heat and salt due to their respective differences in molecular diffusion.

1.3.6   Taylor frozen field hypothesis

The measurement of turbulence is primarily made by profiling through the water, either vertically with free-falling instruments, or horizontally with self-propelled or autonomous vehicles. An alternative case is through moored instrument, where it stands passively as the flow passes over the sensors. In all cases, to obtain a coherent measurement of the local turbulence field, the time series (or frequency spectra) must be converted into a spatial series associated with wavenumber spectra. The notion that time series of any turbulent quantity can be converted into a spatial sequence is based on the Taylor Frozen Field Hypothesis. The term frozen field refers to the assumption that spatial structures do not evolve during the time interval of profiling[13].

The sequence is

$$f(t) \rightarrow f(z = Wt), \tag{1.47}$$

where z and W are the depth and speed of profiling, respectively. The conversion to an along-path gradient using gives

$$\frac{\partial}{\partial t} = W \frac{\partial}{\partial z} \tag{1.48}$$

For example, a length scale of $\mathcal{O}(1\ \text{m})$ is sufficient to estimate ϵ in an eddy of size l, whose time evolution is $(l^2/\epsilon)^{1/3}$. Even if the dissipation is very large, the time scale of the evolution of eddies is many tens of seconds. Therefore, for profiling speeds faster than 0.1 ms^{-1}, the turbulence is essentially frozen.

1.3.7   Spectra of velocity fluctuations

The wavenumber spectrum of velocity fluctuations, was first addressed by Kolmogorov (1968). He proposed that, for steady and isotropic turbulence at scales smaller than those of the largest energetic eddies, l, the spectrum of velocity fluctuations, S, should depend on ϵ and the wavenumber, k, in units of radm^{-1}. The total variance of a spectrum of velocity fluctuations is

$$\overline{u'^2} = \int_0^\infty S(k)\ dk. \tag{1.49}$$

The spatial range $l^{-1} \ll k \ll L_K{}^{-1}$ is called the inertial subrange. In this range, the velocity fluctuations do not depend on the details of the energy containing scales, but on the transfer of kinetic energy from the large scales, passing through L_O, to the dissipating scales. The velocity fluctuations are not dampened by viscosity in the

---

[13]The concept is identical to the synoptic field commonly used in oceanography

inertial subrange. Viscosity only becomes important at scales $k > L_K^{-1}$, or the viscous range, where the energy starts being dissipated into heat.

The universal form for the energy spectrum based on Kolmogorov theory is

$$S = A\epsilon^{2/3}|\mathbf{K}|^{-5/3}, \tag{1.50}$$

where A is the Kolmogorov constant and $\mathbf{K} = (k_1, k_2, k_3)$ is a three-dimensional wavenumber. In isotropic turbulence, a one-dimensional wavenumber spectrum can be derived from the three-dimensional by integrating over the range of the other two components. The $k^{-5/3}$ refers to the shape of the inertial subrange, characterized by a $\sim$-5/3 slope (Fig. 1.8). At $k > L_K^{-1}$, the range of wavenumbers affected by viscosity, the spectrum rolls off more rapidly than $\sim$-5/3.
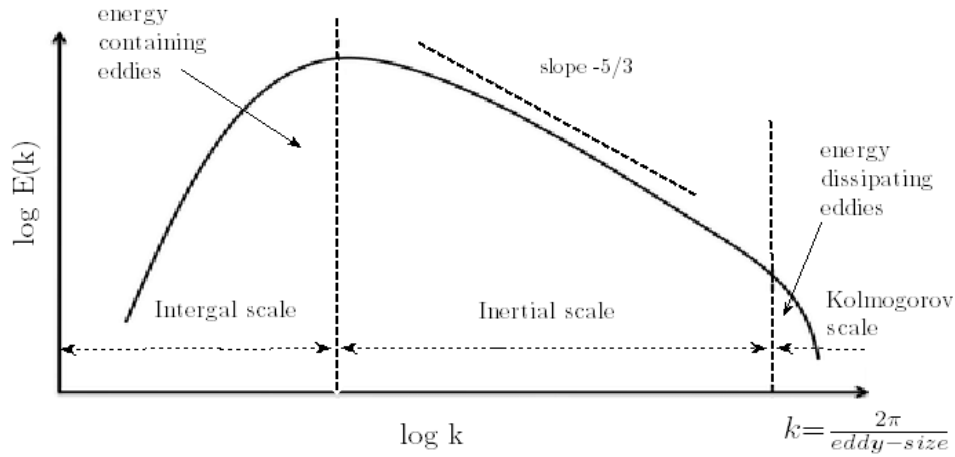
Fig. 1.8: A sketch of the Kolmogorov wavenumber spectrum of velocity fluctuations. The inertial subrange is the mid spectrum range with a $\sim$-5/3. In the dissipation range, the energy rolls off rapidly due to viscous dissipation. From Sinha (2013).

1.3.7.1 Nasmyth spectrum

Nasmyth (1970) obtained a very large data set in the Discovery Passage, that spanned a wide range of ϵ. By gathering the data, he was able to unify the variability in dissipation rates into a single non-dimensional spectrum of velocity fluctuations in the direction of profiling. The Nasmyth spectrum for velocity fluctuations, or shear variance, was later published by Oakey (1982).

The non-dimensional form of Nasmyth spectrum is given by the empirical equation

$$\Psi_N = \frac{8.05(kL_K)^{1/3}}{1 + (20.6(kL_K))^{3.715}}. \tag{1.51}$$

The spectrum describes the behavior of velocity fluctuations towards small scales, which generally shows that the effects of viscous forces became significant at non-

dimensional wavenumbers of ∼10 cpm (Fig. 1.9). This is consistent with the notion that viscosity becomes important at scales comparable to, and smaller than, L_K.
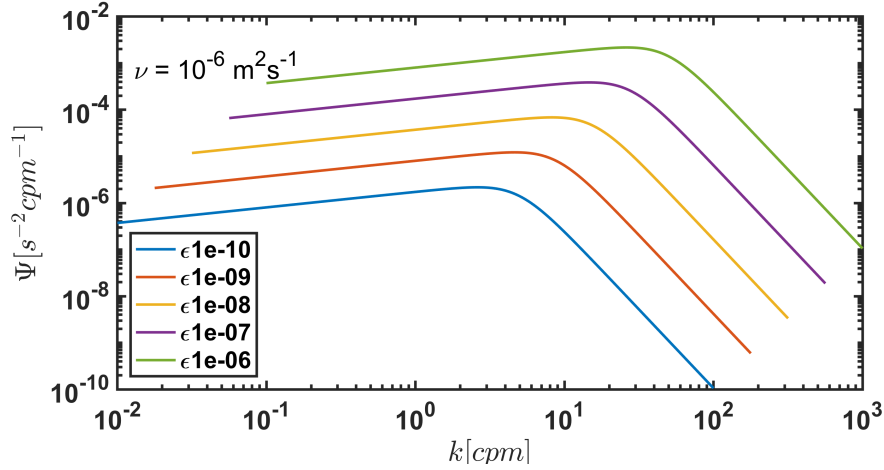
Fig. 1.9: Nasmyth spectra for different values of ϵ; the increase of dissipation causes the increase in spectral variance, caused by the increase in velocity shear.

By using the spectral notation developed by Nasmyth, it is possible to estimate the rate of dissipation of TKE from the integration of the measure micro-scale velocity fluctuations spectrum using

$$\epsilon = \frac{15}{2}\nu \int_{k_1}^{k_2} \Psi(k)dk, \tag{1.52}$$

where the integration is made between the wavenumber k_1 and k_2. Deriving the velocity shear variance in the spectral domain offers advantages over calculating the variance in the spatial domain. (1) The measured spectrum can be compared to the Nasmyth theoretical form for quality assessments, (2) the noise at high wavenumbers can be eliminated by reducing k_1 and (3) it is easier to identify contamination by possible vibrations during the measurements in the spectral domain.

Chapter 2

Motivation, survey areas and methodology

2.1   Why study turbulence?

Since it began with Kolmogorov's theory and laboratory studies at Cambridge University, the study of ocean turbulence has attained a large degree of importance nowadays. As the field improved considerably, measurements are now conducted by researchers in many countries. The growing population by the coastal seas have imposed great stress on the marine environment, increasing the requirement of a better management as the exploration of resources enhanced. Pollutants and nutrients are rapidly dispersed in the oceanic environment due to turbulence, and the magnitude of turbulent mixing exerts large control on the growth and behavior of small marine organisms. The ambient turbulence leads to an intricate network of connected processes in different areas of the deep and coastal ocean as shown in section 1.2 and summarized in Fig. 2.1.

A relatively recent study from Gargett (2003) demonstrate that small-scale turbulent diffusion in the deep ocean affects the overall ocean circulation, with potential implications for the climate change. In addition, the transfer of momentum, heat, and gases across and near the ocean surface, is largely controlled by turbulent processes. Therefore, the small-scale turbulence can have substantial effects on climate (e.g., Munk and Wunsch, 1986).

The understanding of how turbulence is produced, its nature and effects is of considerable importance in practical applications. As mentioned previously, its most important property is that, by generating relatively large gradients of velocity at very small scales, turbulence promotes viscous dissipation that transfers its kinetic energy into heat. In the ocean the amount of heat produced by viscous friction is rather insignificant to its dynamics. What is most important, however, is not the amount of heat generated

34
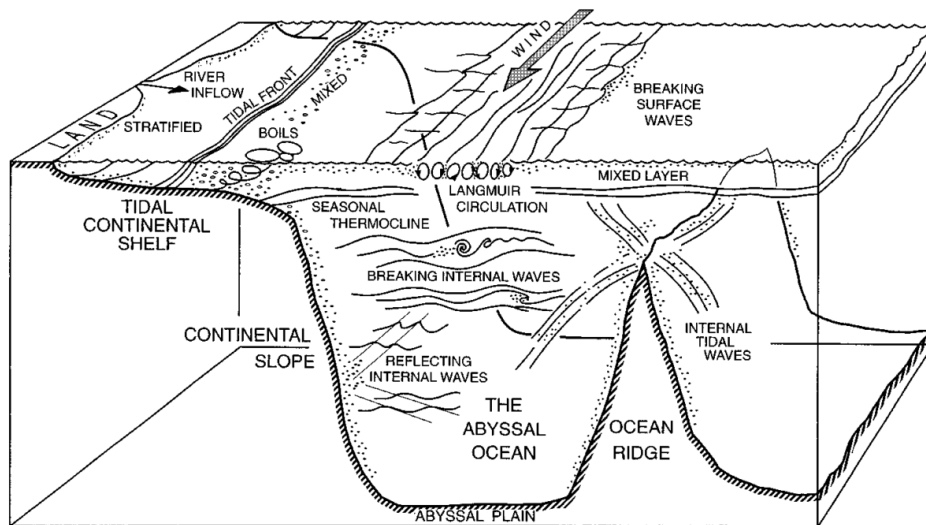
Fig. 2.1: A sketch summarizing the processes related to turbulent mixing From the coastal ocean to the deep ocean. From Thorpe (2004).

by turbulence, but the loss of energy through dissipative processes (Thorpe, 2004). The energy lost in the dissipation scales is crucial to maintain the ocean dynamics stable. Mesoscale motions may present characteristics of turbulence and play a key role on the overall ocean circulation and climate in the dispersion of momentum, heat, and nutrients. However, the origin of instabilities that lead to turbulent mixing and heat loss is at the micro-scales.

According to Lueck et al. (2002), for one to described correctly the ambient turbulence, three main elements are necessary: (1) a sensor or probe capable of fast-response sampling of the parameters of interest, (2) electronic circuitry that provide amplification and filtering of the signal captured by the sensor or probe (as micro-scale measurements may present high levels of noise) and (3) a platform (or body of the instrument) to move the sensor or probe through the water column. In the study of turbulence, effort has been put through the development of reliable and robust techniques and instruments to operate in the severe ocean environment. A wide variety of sophisticated instrument systems are used to profile horizontally and vertically, through the marine environment, but it all started with a horizontal profiler, a paravane converted into a towed vehicle developed by Grant et al. (1962), which produced the very first ocean turbulence measurements (Fig. 2.2).

The first vertical profiles of ocean turbulence were reported in Gregg (1977), made by the research group of Charles Cox at the Scripps Institute of Oceanography in the mid 1960. The profilers were equipped only with temperature sensors, the hot-film anemometer and thermistors, because shear probes had not yet been fully developed. Measurements of dissipation from velocity fluctuations were only possible after the mid 1970, with the development of the air-foil probe, or shear probe, by Ribner and Siddon

Fig. 2.2: The towed paravane used by Grant et al. (1962) to obtain the first records of micro-scale turbulence in history.

(1965), and its subsequent adaption for ocean use by Osborn (1974) (Fig. 2.3). The air-foil probe was a great advance in velocity turbulence measurements in the ocean and still is commonly used in turbulence observations nowadays. It provides the principal means of measuring turbulence at micro-scales in the stratified ocean. The probe is composed of a piezoelectric crystal, protected from direct contact with seawater by a moulded rubber tip. The crystal yields electrical signals proportional to the changes in one component of the lateral force. The force to which the probe responds is the one caused by the relative lateral water speed produced by the turbulent eddies generated as the probe passes through the water column. A shear probe is calibrated to convert the rate of change of the force into the rate of change of the component of the relative lateral velocity of the water, i.e., shear variance. To resolve the spatial scales of the dissipating eddies, measurements are made at frequencies greater than 200 Hz, corresponding to horizontal distances of about 2.5 to 10 mm (Thorpe, 2007). After the establishment of the air-foil probe, a large number of different vertical profilers were created by research groups in Canada and USA, followed by profilers developed in Europe and Japan (Lueck et al., 2002).

As stated in Chapter 1, it is not possible to represent the details of turbulent motion within large-scale numerical models, as the fluctuations terms can not be reproduced numerically. To represent the effects of turbulence, a parametric form of quantities is required to "close the problem". When deriving a parametric representation it is
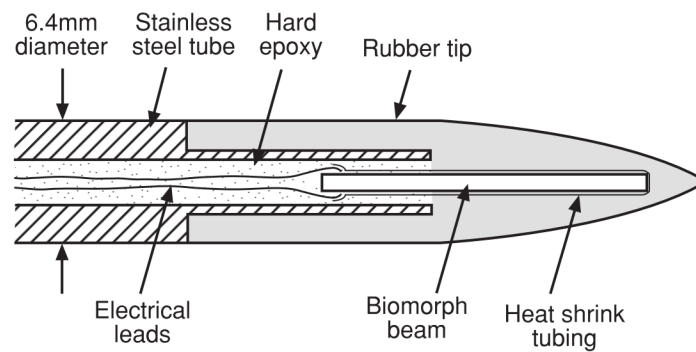
Fig. 2.3: Structure of the air-foil probe used in oceanic turbulence designed by Osborn (1974). From Gregg (1999)

essential to be aware of the processes that contribute most to turbulence and that the model responds correctly to these processes. Failure to include such measures may be particularly dangerous, as the incorrect representation os fluctuations may transfer the associated errors exponentially at larger scale in the inverse energy cascade. This problematic remarks the importance of field observations in the study of turbulence. Observational data provides a base for turbulence models, leading to more reliability on the reproduction of the non linearity that lead to turbulence. Even considering the significant advances in turbulence studies, the oceans are still under sampled and many of the processes that lead to mixing are yet to be fully understood.

Leaving aside the fact that the study of turbulence is hugely interesting, one of the major motivations of this thesis is an attempt to initiate studies of turbulence and mixing in Brazil. The two regions explored in this thesis, namely the Southern Brazilian Shelf (hereafter SBS) and the Vitória-Trindade Ridge (hereafter VTR), are of major importance, not only in terms of oceanographic studies, but in resources exploitation and biological preservation. Both, however, up to the day of the study herein, have no description regarding turbulent mixing processes.

2.2 Objectives

2.2.1 Main

Quantify and describe the processes related to turbulent mixing in the SBS and in the VTR.

2.2.2 Specifics

- Estimate the magnitude of turbulent mixing in the SBS in areas influenced by freshwaters using microstructure temperature;

- Verify the buoyancy-driven effects on diffusivity in the La Plata plume interface with oceanic waters;

- Obtain estimates of the turbulent mixing in the surface mixed layer and in the ocean interior in the VTR;

- Identity the source of a subsurface mixing patch found in the vicinity of a specific seamount in the ridge.

2.3 Hypotheses

- SBS $\Rightarrow$ The large spatial scale buoyant plume from La Plata River reduces the magnitude of vertical mixing in the continental shelf.

- VTR $\Rightarrow$ Flow-topography interactions are capable to enhance the local levels of turbulent mixing at specific topographic features


2.4 Study areas

2.4.1 Southern Brazilian Shelf

The SBS is the continental shelf area located between the latitudes of 28°S and 34°S, from the locations of Chuy to near Sta. Marta Cape, in the southwestern limb of the South Atlantic Ocean. This area presents a highly variable hydrographic distribution and circulation patterns, modulated by the seasonal variation of the wind field, being NE during spring and summer and SW during autumn and winter (Soares and Möller, 2001).

The primary source of freshwaters in the SBS is the La Plata River estuary. The input of a large amount of low salinity waters in the coastal zone, with an historical average of, approximately, 22500 m^3s^{-1}, has a strong impact on the local dynamics, as it creates strong horizontal and vertical density gradients (Guerrero et al., 1997). A secondary source of freshwater is the hydrological basin of Patos Lagoon. Its estuary, the only connection between a 200000 km^2 basin and the ocean, drains waters from several rivers from south of Brazil and north of Uruguay. The mean freshwater discharge of Patos Lagoon estuary is 2400 m^3s^{-1} with maxima of m^3s^{-1} during El niño years (Moller et al., 2001). The Patos Lagoon outflow over the SBS is highly surpassed by the La Plata River and usually the Patos Lagoon plume is embedded at La Plata River plume (Burrage et al., 2008).

The La Plata River outflow as coastal plume waters, namely Plata Plume Water (PPW), spreads along the coasts of Argentina, Uruguay and Brazil, mixing with other
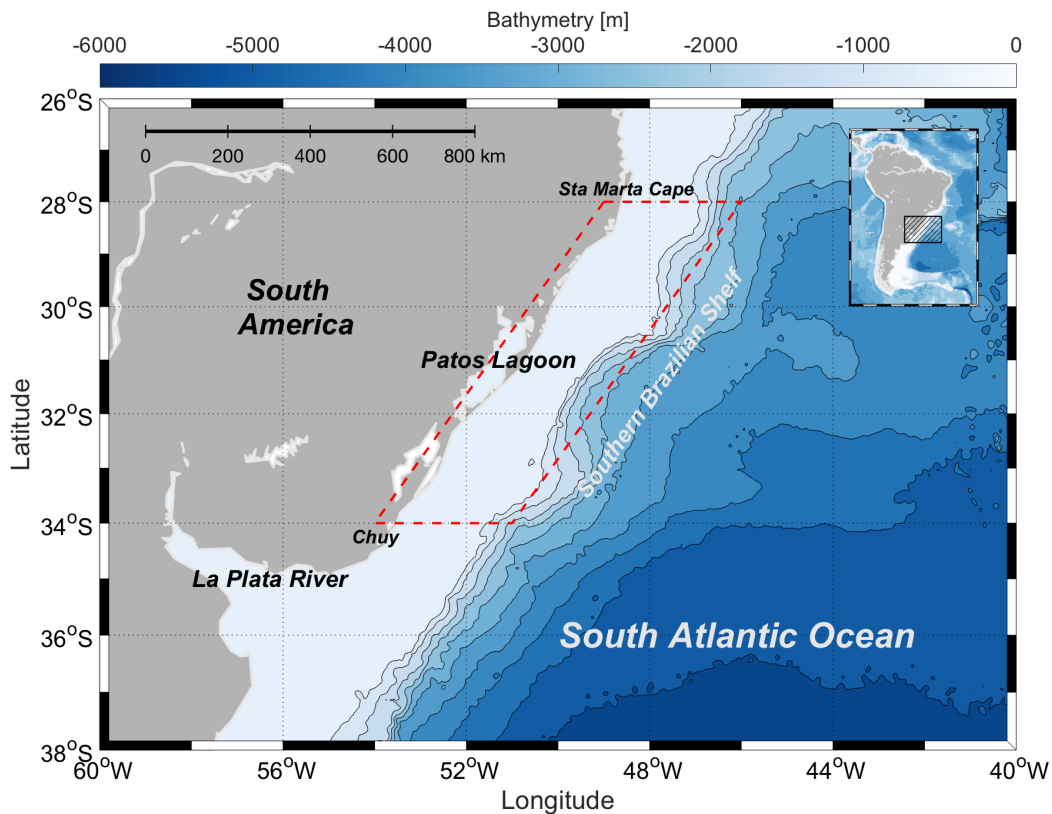
Fig. 2.4: The SBS region and vicinities. The red dashed rectangle is the corresponding area of the shelf. The La Plata River estuary is located outside the limits of the SBS, although its outflow, in the form a large-scale estuarine plume, plays a major role on the circulation pattern of the area. The Patos Lagoon estuary represents a second and minor source of freshwaters when compared to the La Plata estuary.

water masses from the Malvinas and Brazil Current (Möller et al., 2008). The low density plume interacts with the waters transported southward by the Brazil Current (hereafter, BC), namely the Tropical (TW) and the South Atlantic Central Water (SACW). The mixing between PPW and TW forms the Subtropical Shelf Water (STSW), which occupies subsurface layers, mainly at the interface between the plume and oceanic waters. Due to its spatial dimension, which surpass the Rossby radius of deformation[1], the La Plata plume is subject to the Coriolis force, being, therefore, deflected towards north. The northward flow of PPW is nearly geostrophic, and follows along the edge of the coastline as a trapped Kelvin Wave (Pimenta et al., 2005). Although the spatial distribution of PPW over the continental shelf is primarily driven by Earth's rotation, the seasonal wind pattern affects directly the magnitude of the northward/eastward displacement of the plume (e.g., Soares and Möller, 2001; Möller et al., 2008). SW winds induce enhance the northward spreading of the plume, which can reach the vicinities of the Sta. Marta Cape. This northward flow carried by SW winds generate a relatively

---

[1]The Rossby radius of deformation, $L_{Ro} = NH/f$, is the length scale at which rotational effects become as important as buoyancy or gravity wave effects. For a near-geostrophic eddy field, L_{Ro} is the length scale that dictates the flow.

slow but highly energetic coastal current, which flows in the opposite direction to the BC. This northward current was reported in the literature as the Brazilian Coastal Current (BCC) (De Souza and Robinson, 2004), Conversely, NE winds act to reduce the northward displacement of the plume and spreading it towards the shelf break through Ekman transport, allowing a larger presence of warm salty waters near coastal areas and inducing upwelling near Sta. Marta Cape (Campos et al., 2013). The schematic diagram in Fig. 2.5, from Möller et al. (2008), summarizes the circulation pattern associated with summer and winter in the SBS
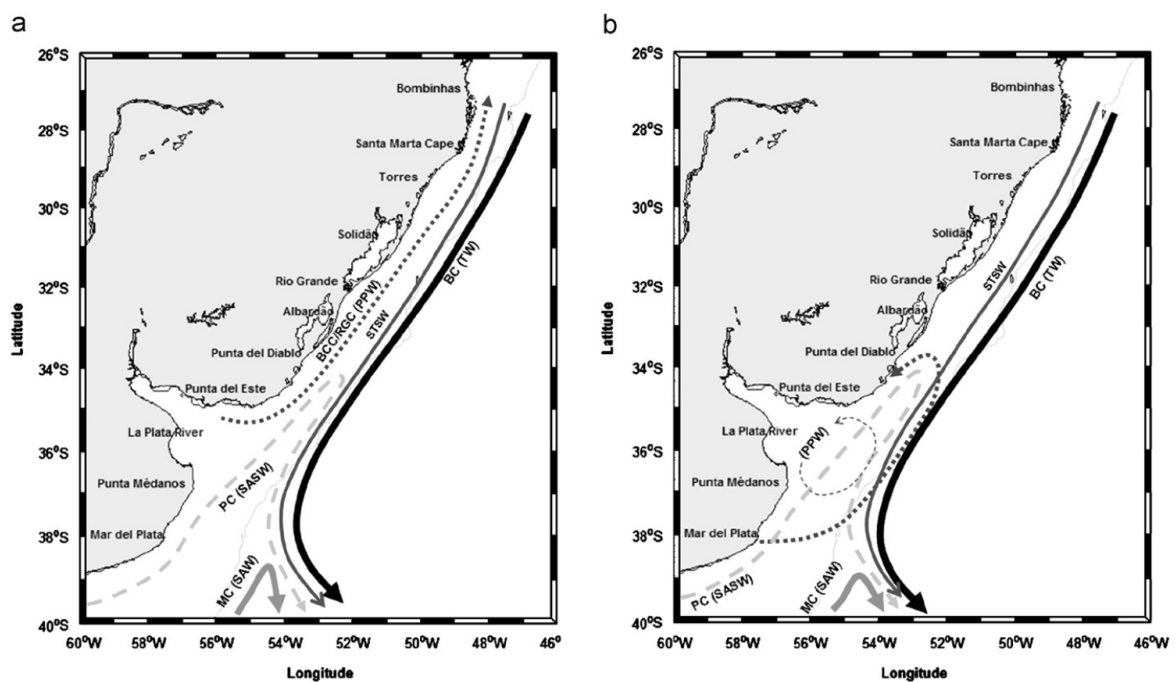
Fig. 2.5: Schematic representation of water masses and currents for (a) winter and (b) summer in the SBS. The BCC is also known in the literature as Rio Grande Current (RGC) (Zavialov and Möller, 1998). PC stands for Patagonian Current, which transports SubAntarctic Shelf Waters (SASW) from southern latitudes into the shelves off Argentina and Uruguay. MC stands for Malvinas Current, which transports SubAntartic Waters (SAW) to the location of the confluence. From Möller et al. (2008).

The presence of the low salinity waters above oceanic waters, induces the formation of an inverted thermocline profile, first observed by Castello and Möller (1977). This is a ubiquitous feature in the area affected by PPW in the SBS, mainly nearshore, where colder waters remain at the surface layer due the lower density of plume waters.

The southward flow of the BC has also a significant influence on the SBS circulation. This boundary current flows along the shelf break and outer shelf areas of the SBS, as it transports warm-salty tropical waters southward (Matano et al., 2010). The low frequency variability associated with the intrusion of tropical and subtropical waters in the outer shelf is mainly controlled by the BC (Soares and Möller, 2001), which has its influence increased during austral summer, reaching its maximum southward displacement near 39°S (e.g., Olson et al., 1988; Goni and Wainer, 2001).

The seasonal variability is the most important in the SBS, associated with the wind patterns and river discharge. However, the interanual scales akin to ENSO oscillations has effects on the mean discharge of the nearby rivers (Robertson and Mechoso, 1998; Marcelo Acha et al., 2008). The synoptic meteorology of the region is highly conditioned by the frontal systems associated to cold air masses moving from the southern Pacific Ocean toward the Atlantic, with a periodicity of 3 to 10 days (Stech and Lorenzzetti, 1992). Studies that evaluate the importance of high frequency events (e.g tidal effects) are practically nonexistent for the continental shelf, being restricted for the estuarine areas. The reason for that is the reduced effect of tidal events in the SBS, due to the low amplitude ($>$0.5m) at 32°S and the presence of an amphidromic point for the semidiurnal component M_2 (De Mesquita and Harari, 2003).
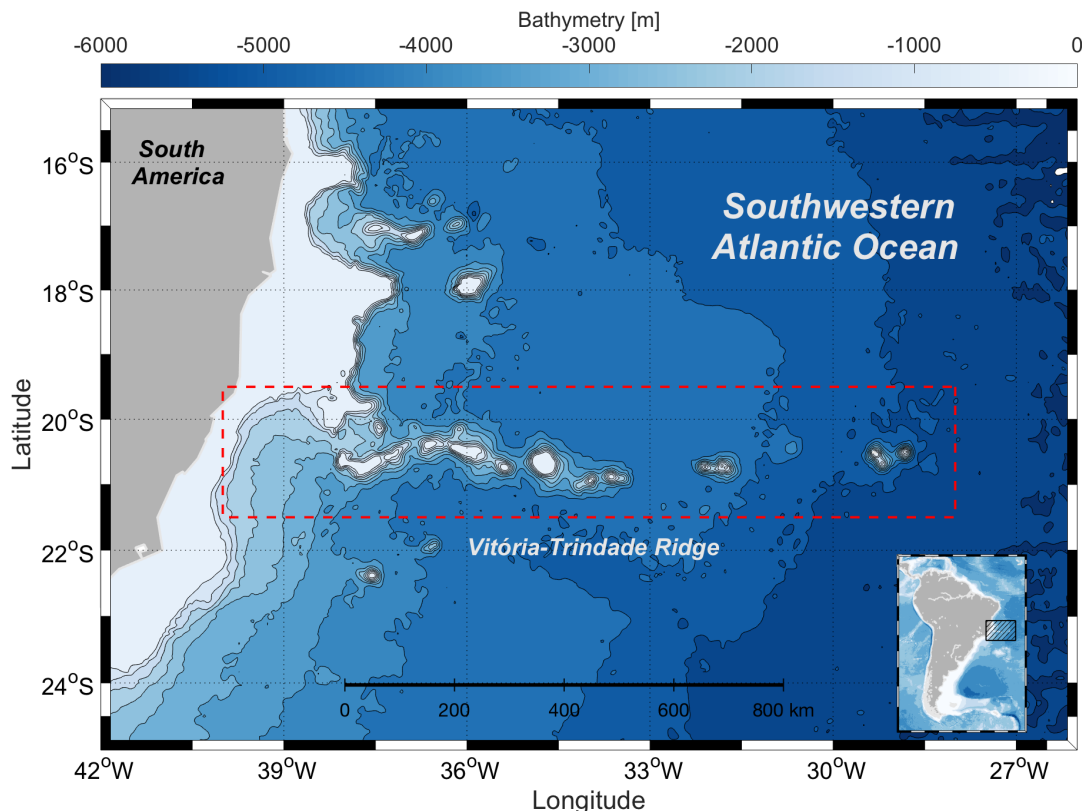
2.4.2 Vitória-Trindade Ridge

The VTR is located in the southwestern Atlantic Ocean at the vicinity of the eastern Brazilian continental shelf (Fig. 2.6). The ridge extends practically zonally about 1000 km towards offshore around the latitude of 21°S, and is composed of more than 30 conical seamounts and banks, having possible the most complex bottom topography in the in the southwestern Atlantic Ocean (Motoki et al., 2012).

The circulation pattern in the site of the VTR is associated with the interaction of the BC with the complex bottom topography (Soutelino et al., 2013). North of the region, the southern branch of the South Equatorial Current (sSEC) bifurcates, originating the southern limb of the BC (Stramma and England, 1999). When reaching the area of the ridge, the BC presents a complex vertical structure as it flows southward along the continental slope (Fig 2.7).

Intense mesoscale circulation is observed in the region due to instabilities induced over the flow of the BC (Soutelino et al., 2011). In the upper 100 m, the BC flows southward along the shelf break in the westernmost part of the basin, being sometimes displaced offshore due to the interaction with topographic features (Da Silveira et al., 2000; Soutelino et al., 2013). When reaching the continental shelf, the circulation is mostly composed of mesoscale eddies. Some of the coherent eddy-like structures are quasi-permanent features in the region, such as the Ihéus Eddy at 15.5°S, the Royal-Charlotte Eddy at 17°S and the Abrolhos Eddy at 19°S (Soutelino et al., 2013). South of 20°S a cyclonic eddy, the Vitoria Eddy, is formed at the shelf-edge south of the Abrolhos Bank (Arruda et al., 2013; Schmid et al., 1995). The sSEC is also the preferential path of propagation of the Agulhas rings as they cross the South Atlantic (De Ruitjer et al., 1999). Therefore, the VTR may be the first contact point of these rings with the western portion of the basin.

Most of the region is composed of oligotrophic waters, as the surface layers are

Fig. 2.6: Location of the Vitória-Trindade Ridge in the southwestern Atlantic Ocean. The red dashed rectangle refers to the zonal displacement of the ridge, starting from the Brazilian coast off the Espírito Santo, Brazil extending almost 1000 km offshore.

dominated by warm-salty TW brought by the BC, from surface to about 200 m [Peterson and Stramma (1991)]. Subsurface layers between 400-500 m are mostly composed by nutrient-rich SACW. At deep layers up to 1000 to the bottom, Antarctic Intermediate Water (AAIW) and North Atlantic Deep Water (NADW) can also be found in the area (Stramma and England, 1999).

Instability studies suggest that the vertical shear of the upper portion of the BC transfers baroclinic energy from the mean flow resulting in eddy formation (Soutelino et al., 2013). This feature is one possible indicator that the VTR is a region prone to baroclinic conversion, and hence, generation of internal tides and/or hydraulic jumps. However, up to this date, only the study of Pereira et al. (2005) verified the role of internal tides in the VTR by numerical simulations. Results showed that the interaction of semidiurnal tidal currents, relative to the M_2 component, and the bottom topography of the southern flanks of the Abrolhos and Royal Charlotte banks induces local upwelling of SACW, thus increasing local levels of primary productivity. Moreover, the seamounts of the VTR are known to be hotspots of ecological diversity and are important sites for fisheries, as nutrient delivery in the vicinity of these regions is increased, in contrast to the oligotrophic conditions in the adjacent open ocean (Pinheiro et al., 2015).
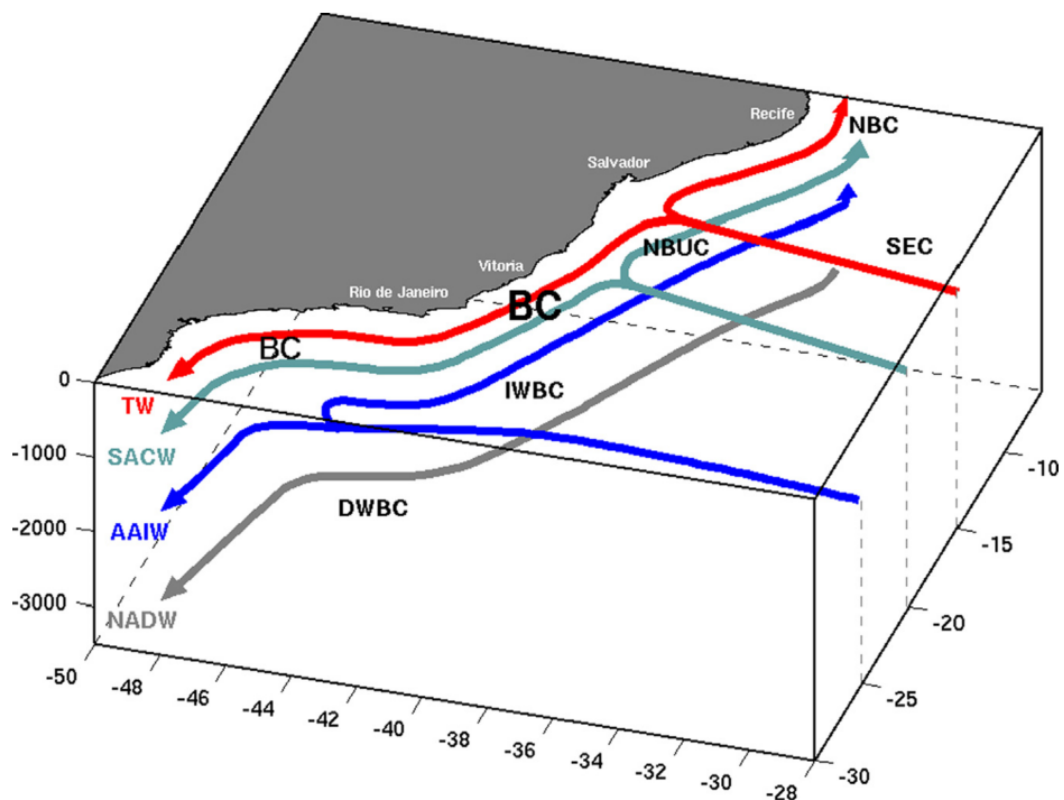
Fig. 2.7: Schematic structure of the BC and water masses in the western Atlantic Ocean made by Soutelino et al. (2013). The vertical structure of the southern branch of the BC when reaching coastal areas assumes a baroclinic structure associated to (1) topographic instabilities and (2) mixing with local water masses. NBC corresponds to the northern branch of the BC. The Deep Western Boundary Current (DWBC) and the Intermediate Western Boundary Current (IWBC) transport Antarctic Intermediate Water (AAIW) and Northe Atlantic Deep Water (NADW), respectively.

2.5 Material and methods

2.5.1 Cruises details

The first dataset was obtained in the SBS in two cruises of opportunity onboard R.V. *Atlântico Sul*, from Federal University of Rio Grande, Brazil. The first one was carried out from June 2 to 11 and the second one from June 30 to July 8, both in 2015. The cruise tracks were planned as transects from the coast to the shelf break, according to time limitations and sea conditions. From the first cruise, only hydrographic data is presented in this thesis, obtained in a cross-shelf transect carried out near the location of Rio Grande. The turbulence data for the SBS was collected on the second cruise, in two cross-shelf transects, one close to the Albardão (AL) region and another close to the Sta. Marta Cape (SM) region. Mostly sea conditions were calm during the 2015 cruises, except for a storm event occurred in the second one, on July 3, where strong winds damage the ship and delayed part of the survey. In the SBS survey, hydrographic data was collected mostly underway, but turbulence data was obtained in profiles were

made in 13 stations, 8 in the AL and 5 in the SM transect (Fig. 2.8).
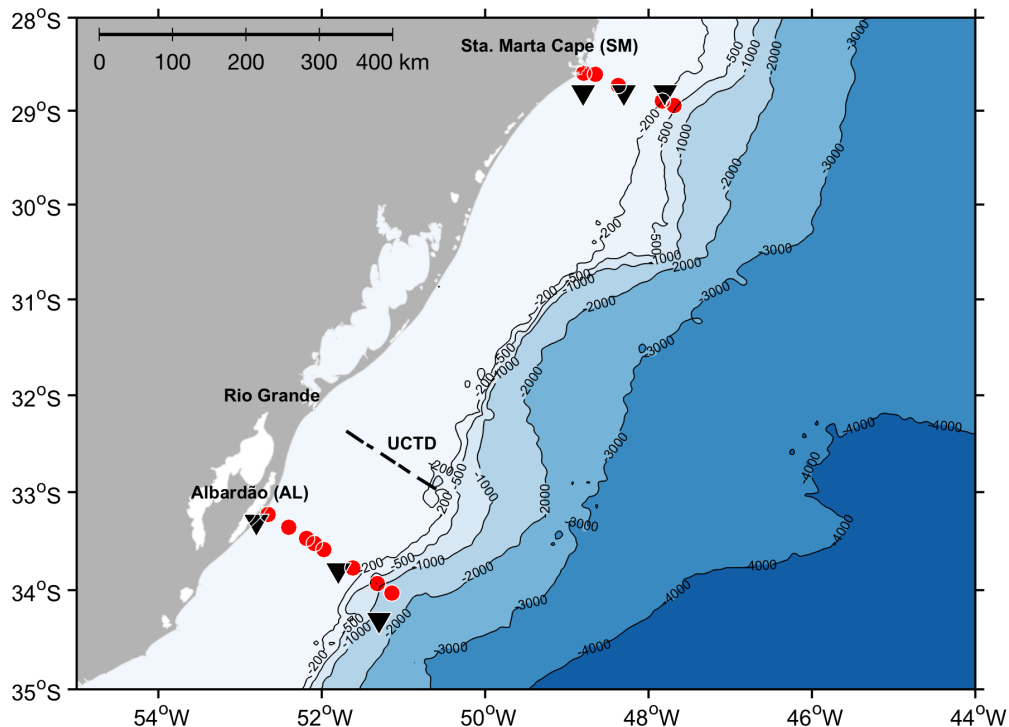
Fig. 2.8: SBS survey map with bathymetric contours from ETOPO2. The red dots are the oceanographic stations made during the second cruise in the region, where microstructure data was collected. Stations were made along two cross shelf transects, at Albardão (AL, 8 stations) and Sta Marta Cape (SM, 5 stations). The black thick lines are the UCTD casts made during the first cruise and the black triangles are the positions where the time series of Q_i and τ_w where taken.

The second data set was collected in the VTR aboard the R.V. *Alpha Crucis*, from University of São Paulo, Brazil, in a cruise from January 25 to February 15 of 2017. The data was obtained along a transect above the main topographic features of the ridge. As expected for a warm and quiescent region, sea conditions were very calm during the time of the survey. Likewise in the SBS survey, part of the data was collected underway, but also obtained in 16 stations scattered along the transect's path (Fig. 2.9).

2.5.2 Microstructure data processing

For both SBS and VTR surveys, all the microstructure data was obtained with a vertical microstructure profiler from *Rockland Scientific* (VMP-250). The instrument is equipped with two shear probes, a SBE7 micro-conductivity probe and a FP07 thermistor, capable of measure velocity shear variance, $\partial u'/\partial z$, conductivity and temperature, respectively, at a 512 Hz sampling rate. For the SBS survey, the shear probes were not available due to technical problems.
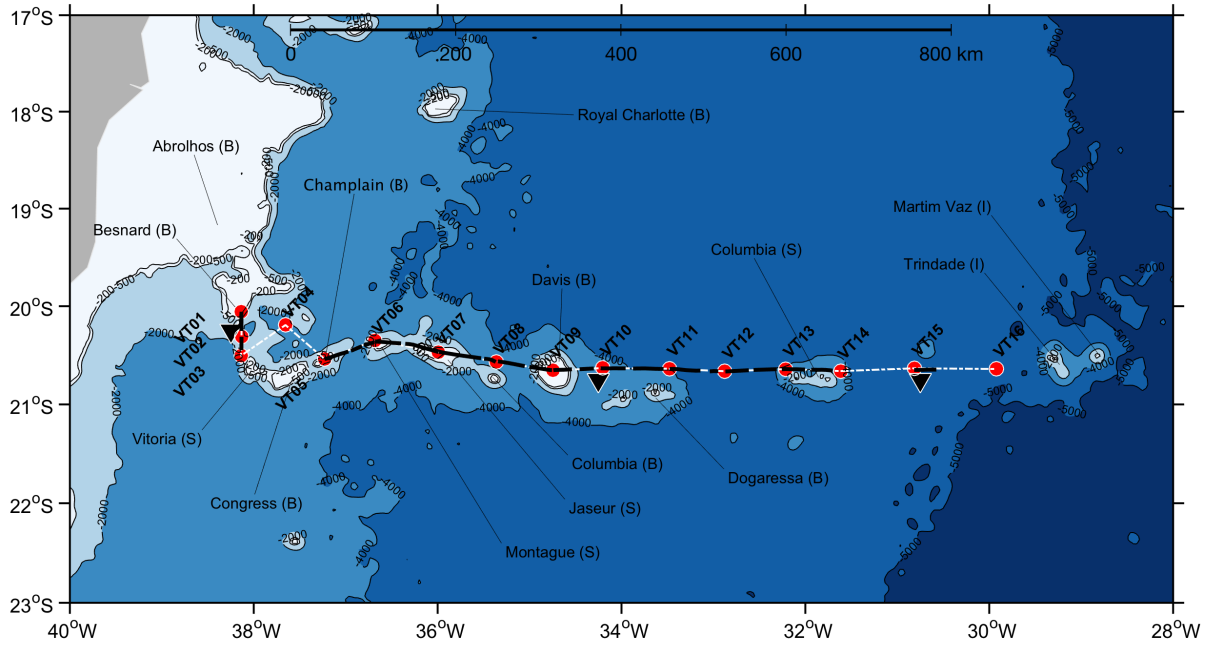
Fig. 2.9: VTR survey map with bathymetric contours from ETOPO2 data. The red dots are the oceanographic stations, black thick lines are the UCTD casts, the point-dashed white line is the transect's path where velocity and bottom topography were obtained continuously and the black triangles are the positions where the time series of Q_i and τ_w where taken. (S) stand for seamounts, (B) for banks and (I) for islands.

For all profiles for both campaigns the instrument was used in downcast mode, descending freely through the water column. For deep casts (i.e., more than 100 m), it was necessary to add more weight to the VMP, in order to avoid increased drifting in deep casts. Although the instrument is equipped with a stability device to promote a smooth descend, significant variability in the instrument drop speed (W) was verified. For all casts, W spanned within $\sim$1-1.5 at the surface to nearly $\sim$0.1-0.2 ms^{-1} at the bottom of the profiles. Although this variability did not affect the quality shear variance data, thermistor data was needed to be corrected with a response function. The response to changes in temperature is limited by the time for heat to diffuse through the boundary layer surrounding the sensor (Gregg and Meagher, 1980), which may be affected by variability in W. Sometimes, a nearly 2 to 3 order magnitude decay at high wavenumbers in the temperature variance spectrum is observed. The temperature gradient spectrum for each depth segment was corrected dividing each spectral segment by the dynamic response function for the FP07 thermistor, following Gregg (1999)

$$H_{FP07}^2 = \frac{1}{[1 + (2\pi\tau/k)^2]^2}, \qquad (2.1)$$

where τ is a drop speed time constant

$$\tau = 0.005W^{-0.32} \quad [s]. \tag{2.2}$$

Due to the high variability akin to microstructure measurements, a recommended procedure during sampling is to drop the instruments at least three times at each location to build ensemble averages of each micro-scale gradient, which increases statistical reliability. Unfortunately, this was only possible in the VTR survey, due to the lack lack of time available in opportunity cruises in the SBS.

As micro-scale data is sensitive to ambient perturbations, the ship's engine was turned off at every single station where the VMP-250 was dropped. Still, in order to avoid possible remnants from the ship's wake, the first 10 m of the profiles were removed in the VTR data. For the SBS, because of the very shallow SML depth found in the areas affected by the La Plata River plume, only the first meter was removed.

The profiles of microstructure data were processed with FFT (Fast Fourier Transform) of 1 and 3 seconds, depending on the local depth, being 1 second for profiles with less than 50 m and 3 seconds for more than 100 m and 50% of overlap, resulting in spectral segments with 257 points each for shallow and 769 for deeper profiles. The length of the FFT segments was based of the instrument drop speed variability. Shallow casts were easier to retain a more or less constant speed along the entire cast. Deeper casts, however, had a reduction in W when reaching deeper portions of the profile. The objective was to maintain the segments with lengths around 1m and to avoid spikes related to large unwanted variability.

The micro-scale shear variance from the shear probes was used to obtain the rate of dissipation of TKE, ϵ, from the integration of the spectrum of velocity fluctuations for each computed segment as

$$\epsilon = \frac{15}{2}\nu \int_{k_1}^{k_2} \Psi_v(k)dk \quad [Wkg^{-1}]. \tag{2.3}$$

The kinematic viscosity of seawater, ν, was measured by the VMP-250. Its typical value is around 1×10^{-6} m^{2}s^{-1}. The brackets denotes an ensemble average. The shear variance is computed by integrating the shear power spectrum from the lowest wavenumber k_1, set to 1 cpm, to the highest k_2, where the shear spectrum has a minimum between the natural spectrum and a high wavenumber peak close to the noise level. If the wavenumber of the minimum energy is smaller than that corresponding to L_K, the integration is extended to k_2 along the Nasmyth spectral form. The segments were processed and ϵ was computed using a series of MATLAB® routines from *Rockland Scientific*.

The micro-scale temperature was used to computed the rate of dissipation of temperature variance, χ_T. The procedure is similar to ϵ, as each temperature spectral

segment is integrated from k_1 to k_2 as

$$\chi_T = 6D_T \int_{k_1}^{k_2} \Psi_T(k) \; dk \quad [K^2 s^{-1}]. \tag{2.4}$$

Each segment is corrected using (2.1) prior to integration. D_T, the molecular thermal diffusivity, is equal to 1.4×10^{-7} ms^{-1}.

The eddy diffusivites of heat, K_T, and density, K_ρ, where calculated with the models of Osborn-Cox and Osborn, respectively, as shown in section 1.3.5, both in units of m^{2}s^{-1}.

The buoyancy flux, B_f was obtained with the turbulent heat flux, F, which is a measured of the vertical flux of heat carried by turbulent motion. F is expressed as

$$F = \overline{\rho c_p w'T'} = -\rho c_p K_T \left\langle \frac{\partial T}{\partial z} \right\rangle \quad [Jm^{-2}s^{-1}], \tag{2.5}$$

where c_p the specific heat of seawater at constant pressure and $\partial T/\partial z$ is the vertical microstructure temperature gradient obtained from the VMP-250. The turbulent buoyancy flux, B_f, is obtained in

$$B_f = \frac{g\alpha F}{\rho_0 c_p} \quad [m^2 s^{-3}]. \tag{2.6}$$

The mixing efficiency, or the flux Richardson number[2] was calculated from the ambient (or observed) flux coefficient, Γ_{obs}, (see section 1.3.5.2) as

$$Ri_f = \frac{\Gamma_{OBS}}{(1 + \Gamma_{OBS})}. \tag{2.7}$$

R_f expresses the efficiency of turbulent mixing by the ratio between buoyancy and shear production, B/S. At fully developed shear-stratified turbulence, Ri_f usually falls between 0.13 and 0.25 (e.g., Osborn, 1980; Ivey and Imberger, 1991). Low values of Ri_f, i.e., close to zero, indicate that shear production is much higher than buoyancy flux. Thus, most of the energy supplied for mixing will be dissipated into heat. Conversely, high values, i.e., close to 1, suggest shear input that is not capable of produce mixing. Based on experimental data, is usually necessary between 15 to 25 % from the input of TKE to overcome buoyancy, as $B \approx 0.2\epsilon$.

In addition to R_f, a parameter that describes the turbulent activity is the turbulent Froude number, Fr_t. It expresses the strength of stratification relative to turbulence,

---

[2]A different notation can be used for R_f, as shown in Kundu et al. (2001). If one considers the signal of B in the energy balance (referred in the book as "buoyant destruction "), associated with TKE consumption (minus) or potential energy loss (plus), a positive R_f indicates a stable environment. Alternatively, a negative R_f indicate tendency towards instability.

being

$$Fr_t = \left(\frac{L_O}{L_T}\right)^{2/3}.$$ (2.8)

Fr_t is a ratio between the Ozmidov length scale and L_T, Thorpe length scale. L_T is the scale of vertical overturns due to density instabilities (Mater et al., 2013), calculated from the observed instantaneous micro-scale density profile from the VMP-250. Discrete density measurements are monotonically sorted to give a gravitationally stable profile. The vertical distance a sample must be moved adiabatically in this process is the Thorpe displacement, δ_T, a signature of mixing in stratified flows. L_T is then calculated as the root-mean-square (RMS) of δ_T as in

$$L_T = \sqrt{\langle \delta_T^2 \rangle} \quad [m].$$ (2.9)

When Fr_t is greater than unity, turbulence is unaffected by stratification. If $Fr_t \gg 1$, the shear input is inefficient in generating mixing because practically all the TKE is being dissipated as heat. Conversely, values of $Fr_t < 1$, indicate that stratification may supress turbulence. High or low values of Fr_t are usually associated with low R_f(e.g., Ivey and Imberger, 1991).

To quantify and determine double-diffusive processes in both SBS and VTR, was calculated the density gradient ratio, R_ρ, with the micro-scale temperature and salinity gradients obtained with the VMP-250. R_ρ was obtained with equation (1.12), and details regarding the nature of diffuse processes are presented in section 1.2.2.2.

2.5.3 Underway data processing

The hydrographic data was collected with an *OCEANSCIENCE* Underway CTD. This instrument samples conductivity and temperature while the vessel is underway with a *SeaBird* probe with 16 Hz of sampling frequency towed by a cable, which is spooled in a winch attached to the stern of the vessel. The UCTD was operated in "tow-yo" mode (e.g., Rudnick and Klinke, 2007) with the depth controlled by the drop time and the vessel speed. The salinity data was smoothed by a 10 scan moving averaged filter and spurious values were removed. In the SBS the underway hydrography was obtained near the region of Rio Grande, where a significant amount of PPW is expected to be found. Moreover, the transect surpasses the plume density front, reaching close to the shelf break (c.f., Fig. 2.8).

In the VTR the instrument collected hydrographic data along the transect between VMP casts, being withdrawn from water at each station. The quasi-continuous data sampling from the UCTD yields a dataset with high horizontal resolution, which allows the detection of very detailed hydrographic features. Therefore, this instrument is ap-

propriate for regions with large hydrographical variations in at relatively small spatial scales. Besides the high spatial resolution, another advantage of this instrument is the fact that sampling occurs while the ship is moving, thus saving valuable ship time.

Estimates of velocity gradients in the location of the La Plata River plume were obtained using horizontal density gradients from the UCTD. In a geostrophic flow, velocity gradients can be obtained from the thermal wind balance as in

$$-f\frac{\partial v}{\partial z} = \frac{1}{\rho_0}\frac{\partial \rho g}{\partial x}, \quad f\frac{\partial u}{\partial z} = \frac{1}{\rho_0}\frac{\partial \rho g}{\partial y}, \tag{2.10}$$

The horizontal density gradients were averaged into a grid with a resolution of 2 km in horizontal and 1m in vertical, chosen in order to retain horizontal gradients associated with the geostrophic balance while removing smaller scale disturbances (Yankovsky, 2006). The resulted velocity gradients and were used to estimated the gradient Richardson Number, Ri_g, with equation 1.4.

Current velocity data was available for the VTR survey only, measured continuously along the vessel's track with a shipboard *RDI* 75 kHz Acoustic Doppler Current Profiler (ADCP), set to measure with 8 m bins, with a blank distance of 16 m plus the ship's draught. During processing, data with less than 70% of quality was removed.

2.5.4 Data from other sources

Hourly time series of net heat flux, Q_i and wind shear, τ_w were calculated with data from the Climate Forecast System (CFSV2) (`https://www.ncdc.noaa.gov/data-access/model-data/model-datasets/climate-forecast-system-version2-cfsv2`). The data was obtained for positions near transects locations (c.f., Fig 2.8 and 2.9), and averaged over three spatial points.

Bathymetry is 2-minute gridded data obtained from ETOPO2 (`https://www.ngdc.noaa.gov/mgg/global/etopo2.html`). This data was used to calculate the topography roughness, r, in the VTR region. r is a measure of the scale of the topographic changes, calculated as the RMS of the bathymetry

$$r = \langle (H - \langle H \rangle)^2 \rangle^{1/2}, \tag{2.11}$$

where $\langle H \rangle$ is the weighted mean of the bathymetry H, given by $\sum w_i H_i$. w_i is a weighting function in the form of a Gaussian filter, $w_i(s) = A\exp(-s_i^2/2\sigma^2)$, with standard deviation $\sigma = l/2$. The sum is carried out over all grid points contained within a circle of radius l, within a radial distance s from the center of a circle. Here, was used $l = 30$ km, following Decloedt and Luther (2010). w_i is applied in order to smooth horizontal spreading of large roughness values calculated at sharp topographic features.

Sea-level Satellite altimetry, or Sea Surface Height (SSH), anomalies were down-